

**KERNFORSCHUNGSZENTRUM
KARLSRUHE**

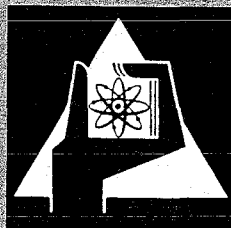
April 1972 – April 1973

KFK 1525

Institut für Angewandte Kernphysik

**Analysis of Surface Reactions and Thin Film Properties
by the Channeling and Backscattering of MeV $^4\text{He}^+$ Ions**

J. Geerk, G. Linker, H. Mann, O. Meyer, S. Petersson



GESELLSCHAFT FÜR KERNFORSCHUNG M. B. H.

KARLSRUHE



Observation of Film Growth Process by Means of Backscattering Technique*

O. Meyer, H. Mann,* and G. Linker

Kernforschungszentrum Karlsruhe, Institut für Angewandte Kernphysik, Germany
(Received 27 December 1971)

Evaporated Sn layers on Si and sapphire substrates were used to demonstrate the applicability of the backscattering technique to measurement of the fraction of covered area, the average thickness of the layer, and the sticking factor for temperatures over the range 77–400 °K. The sticking factor at 293 °K was found to be $\frac{1}{3}$ of that at 77 and 393 °K, and 19% higher at room temperature (r.t.) for Sn on Sn as compared with Sn on Si. At 393 °K the fraction of covered area was found to be about 60% and the average island thickness was in the range 450–1000 Å.

Backscattering of $^4\text{He}^+$ ions in the MeV energy range was previously used to study diffusion processes in thin metal films.¹ In the course of our study of diffusion processes at the Cu-CdTe interface² we were able to demonstrate that this technique is suitable for study of the intermediate stages of growth of thin films. The intermediate stages³ follow nucleation and precede the formation of a continuous film. During the coalescence stage we can measure the fraction of covered area, the average thickness of the layer, and the sticking factor as determined by the substrate material and the substrate temperature. We report here results which demonstrate this application.

Sn was evaporated on Si and sapphire substrates over

the temperature range 77–400 °K. This metal was chosen for its low melting temperature, possibly leading to high surface mobility and facilitating growth of coalescence centers at moderate temperatures ($\sim 100^\circ\text{C}$). The backscattering technique is described in detail elsewhere.⁴

A discontinuous film as a model for the coalescence stage can be constructed by means of evaporation onto a substrate through a wire mesh. The wire separation must be chosen small in comparison with the diameter of the beam (0.6–0.8 mm). For a continuous film the yield of backscattered particles is proportional to the number of atoms/cm². This yield will decrease for a discontinuous film, and the amount of the decrease is

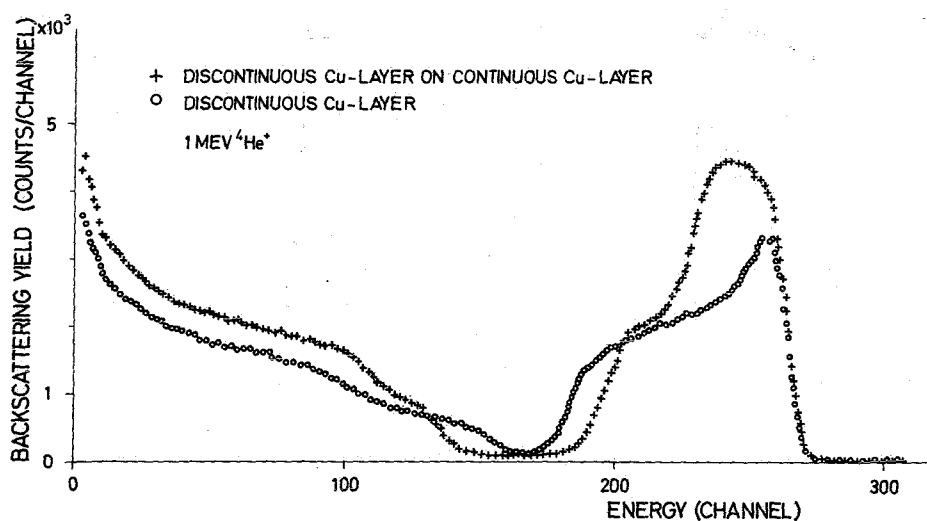


FIG. 1. Energy spectra for $^4\text{He}^+$ ions (1 MeV) backscattered from (x) a discontinuous Cu layer on a continuous Cu layer on Si, and (o) a discontinuous Cu layer on Si.

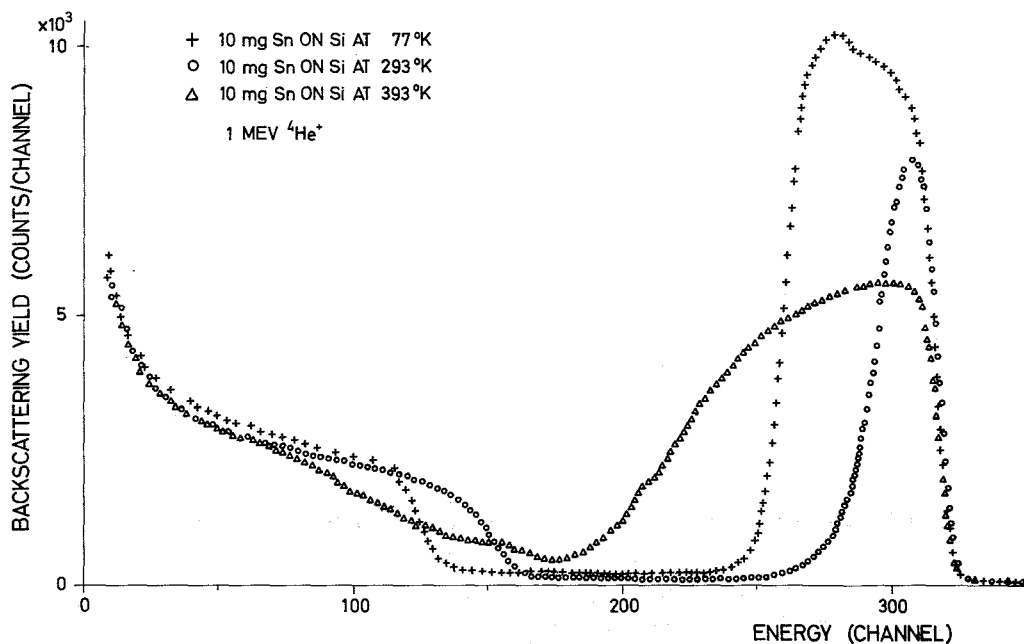


FIG. 2. Energy spectra for ${}^4\text{He}^+$ ions (1 MeV) backscattered from Sn layers evaporated on Si. Equal quantities of Sn were evaporated at temperatures of 77 °K (+), 293 °K (o) and 393 °K (Δ).

proportional to the fraction of uncovered area. Also, inhomogeneity in film thickness will change the shape of the backscattered spectrum. Both effects are illustrated in Fig. 1 in terms of spectra obtained for 1-MeV ${}^4\text{He}^+$ ions scattered from a discontinuous Cu layer on top of a continuous Cu layer evaporated on Si at r.t. The yield at higher values of energy is the same as that for a thick Cu layer, whereas the discontinuous film gives a reduced height toward lower-energy values. In addition, a second spectrum is shown for a single discon-

tinuous film on silicon. The wires of the screen do not provide a sharp mask, and a shadow effect is visible which corresponds to a higher fraction of covered area at smaller layer thickness. The observed dependence of the fraction of covered area on the layer thickness corresponds to the scattering distribution of neutral atoms from the wire, for which analytical expressions could be derived. Thus, Fig. 1 illustrates the applicability of backscattering to the coalescence stage where it is known that islands are formed. The effects of both

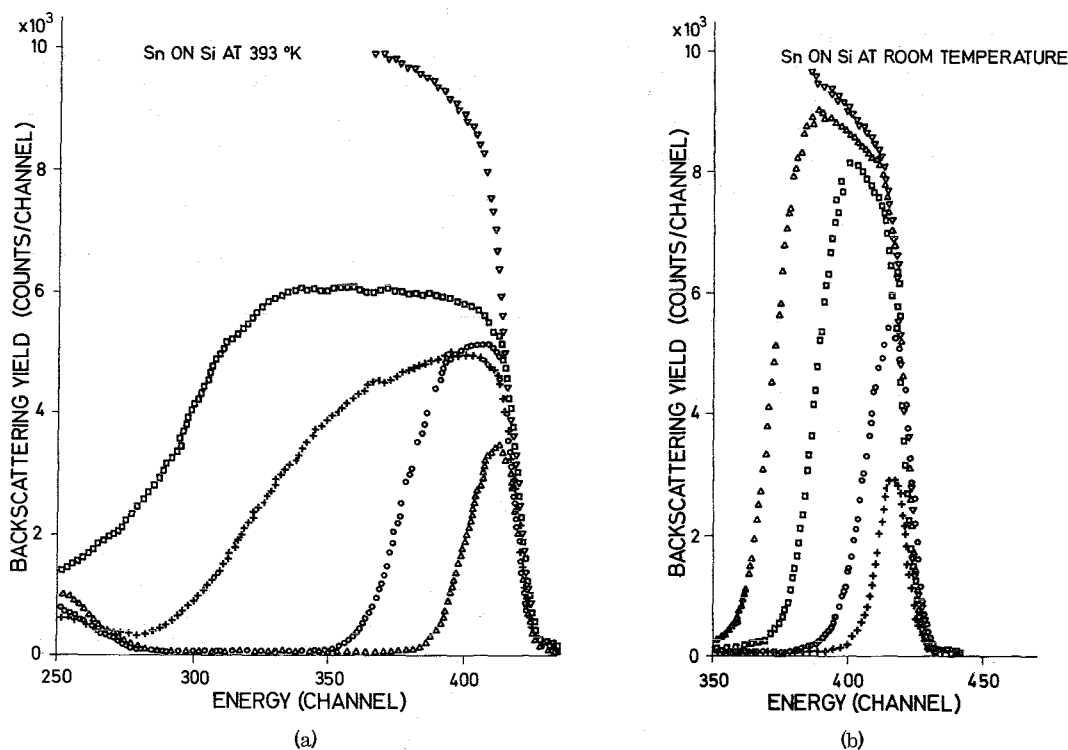


FIG. 3. Portions of energy spectra for ${}^4\text{He}^+$ ions (1 MeV) backscattered from Sn layers evaporated on Si at (a) 393 °K and (b) r.t. In (a) the quantity of Sn used was (Δ) 2 mg, (o) 5.5 mg, (+) 10.0 mg, and (\square) 20.5 mg; in (b) the quantity of Sn used was (\times) 3 mg, (o) 8.5 mg, (\square) 15 mg, and (Δ) 24.5 mg; the higher-energy edge for backscattering from a Sn foil is also shown, (∇).

inhomogeneity of film thickness and cracks (or holes) produced in thin evaporated films during heat treatment may seriously affect diffusion measurements, thereby leading to misinterpretation.

We evaporated equal quantities of Sn onto Si at substrate temperatures of 77, 293, and 393 °K. The results are shown in Fig. 2 in terms of the backscattered spectra. There is a significant reduction in the yield for layers evaporated at the higher temperature, and an increase in thickness obtained at this same temperature. Further, the total number of backscattered particles is substantially lower at room temperature, which shows that the sticking factor is greatly reduced at this temperature. By peak-area integration we find that the sticking factor is the same, to within 6%, at 77 and 393 °K, but at 293 °K it is $\frac{1}{3}$ of that at 77 °K.

The growth of Sn films was studied in terms of the quantity of Sn evaporated. As an example, we show in Fig. 3 the film growth process at substrate temperatures of (a) 293 and (b) 393 °K as the area and thickness increase. Included are the front edges of the backscatter spectra obtained by 1-MeV $^4\text{He}^+$ ions backscattered from a 0.3-mm-thick Sn foil. At 393 °K [Fig. 3(b)] the yield does not come up to that for the foil, using up to 20 mg for the boat load. In contrast, at r.t. about 12 mg, and at 77 °K about 5 mg, produces a continuous film. In our experimental arrangement, we found the following boat loads are necessary to form a continuous film: 3 mg at 77 °K and 12 mg at 293 °K. Far more than 30 mg is required at 393 °K. Using 30-mg Sn, a continuous layer was not formed on the substrate at 393 °K. At 393 °K, it is evident that the fraction of covered area does not increase significantly as the thickness increases. This corresponds to growth of columns where the average thickness increases at a substantially higher rate than the fraction of area covered. In Fig. 3(a) we show the contrasting situation at r.t. where the area covered increases at a rate significantly greater than that for the thickness. This is even more pronounced for the film

growth at 77 °K (not shown), owing to the higher sticking factor at this temperature.

When a sapphire substrate, instead of Si, is used at 393 °K there is a slightly higher concentration of thicker island regions as determined from the shape of the lower-energy portion of the spectrum. We also find that after a continuous layer is formed, the sticking coefficient increases by 19% at r.t. for Sn on Sn as compared with Sn on Si.

Some information on island shape is obtained from the curves in Fig. 3. For example, for Sn evaporated on Si at 393 °K the island shape is approximately rectangular up to an average thickness of 450 Å. With increasing thickness up to about 1000 Å the shape is more rounded, and becomes rectangular again at about 1400 Å. A flat top is expected for thicker layers.

Some attempts were made to observe coalescence and continuity for thin Sn layers by post-heat treatments and by changing the angle of incidence during evaporation, but more work will be done on this topic.

Detailed understanding of film growth processes has been obtained in the extensive studies using electron microscopy. The backscattering technique does not replace electron microscopy, but provides a simple and quick means for obtaining quantitative information on important growth parameters.

The authors wish to acknowledge the assistance of H. Eberle in sample preparation.

*On leave of absence from Argonne National Laboratory, Argonne, Ill. 60439.

¹A. Hiraki, M.A. Nicolet, and J.W. Mayer. *Appl. Phys. Letters* 18, 178 (1971).

²H. Mann, G. Linker, and O. Meyer (unpublished).

³See, for example, K.L. Chopra, *Thin Film Phenomena* (McGraw-Hill, New York, 1969).

⁴J.W. Mayer, L. Eriksson, and J.A. Davies, *Ion Implantation in Semiconductors* (Academic, London, 1970).

Handwritten text in the upper middle section of the page, consisting of several lines of cursive script.

Handwritten text in the middle section of the page, continuing the cursive script.

Handwritten text in the lower middle section of the page, continuing the cursive script.

Handwritten text at the bottom of the page, possibly a signature or concluding remarks.

OXIDATION OF LEAD BY LOW ENERGY O_2^+ BOMBARDMENT

J. GEERK and O. MEYER

Kernforschungszentrum Karlsruhe, Institut für Angewandte Kernphysik, Gesellschaft für Kernforschung mbH, 75 Karlsruhe, Germany

Received 24 January 1972; revised manuscript received 3 March 1972

Evaporated lead layers have been oxidized by bombardment with low energy oxygen ions. The oxidation process is caused by oxygen diffusion as determined with backscattering techniques ($^4\text{He}^+$ ions, 1.5 MeV). The activation energy for oxide forming was found to be 1 eV. Lead monoxide has been formed; the ratio of oxygen to lead atoms close to the surface was found to be about 1.

1. Introduction

Thermal oxidation of lead below its melting point has been studied in detail in the range 90–548 K¹⁾ by monitoring oxygen pressure, and also by use of vacuum microbalance techniques in the range 500–580 K²⁾.

Implantation of oxygen ions with energies in the keV-range has been extensively used to produce oxide layers^{3,4)} with thicknesses of 1000–10000 Å. The present study is concerned with a new method of oxide preparation. Here the surface of evaporated lead layers was bombarded with oxygen ions in the eV-range at energies low enough to avoid substrate sputtering, in order to form oxide films that are thin, homogeneous and continuous. Such films are of considerable interest for applications in electronic devices including superconducting tunneling diodes.

Backscattering of light, i.e., $^4\text{He}^+$ ions in the MeV-range was used here to study the oxidation process. This analysis method is a well-known technique for study of composition and diffusion effects in thin films⁵⁻⁷⁾. As an advantage over the above mentioned analysis methods it also provides a direct measurement of the concentration profile of diffused oxygen ions.

2. Experimental

O_2^+ ions were produced in a HF source and extracted with 12 keV external potential. After focusing with an einzel-lens system the beam entered a deflecting magnet. The analysed beam of O_2^+ ions was then focused with an electric quadrupole lens and allowed to pass through a 6 mm diameter hole into the target chamber. This hole acted as a differential-pumping diaphragm

between the target chamber and the beam production and formation system. In the backable target housing a pressure of 10^{-8} torr could be maintained with a turbo-molecular pump. The pressure decreased to 10^{-7} torr, when a beam of $100 \mu\text{A}$ was fed into the target chamber. In the target chamber the beam was retarded to energies in the eV range by means of a deceleration lens system in front of the heatable and movable substrate holder. The final energy of the ions could be varied between 0 and 1000 eV without serious deterioration of the focus. Before reaching the target the beam passed through a mask so that only the central part of the beam could strike the target. In this way a homogeneous incident beam spot of 4 mm diameter was achieved. The total charge was monitored with an integrator; the same dose rate was used in all experiments.

Pb was evaporated at 10^{-5} torr on highly polished rectangular carbon substrates. These targets were mounted on the substrate holder for irradiation. $^4\text{He}^+$ ions of 1.5 MeV from a 3-MeV Van de Graaff generator were used for the backscattering experiments. The beam current was measured with an integrator; the target was shielded by means of a Faraday cup in order to suppress secondary electrons. The energy distribution of the backscattered $^4\text{He}^+$ ions was measured with a surface barrier detector; the electrical signal from this detector was amplified and stored in a pulse-height analyzer. The linear response of the nuclear particle detector provides a fixed energy-per-channel. Mass and energy calibration was performed by backscattering from thin layers composed of different elements (e.g., Si, O, Pb). The $^4\text{He}^+$ beam diameter was about 1 mm, which is small in comparison with the diameter of the oxide-layer area on the lead. Measurements were performed on the oxidized spots, and directly beside them, in order to avoid or observe possible effects due to film inhomogeneities, and also to correct for oxidation during storage.

3. Analysis

As an example the most important features of a backscattering energy spectrum for 1.5 MeV $^4\text{He}^+$ ions scattered from a 1500 \AA thick lead layer are shown in fig. 1 before and after bombardment with 44 eV O_2^+ ions. The peak in the channel range between 370 and 450 is produced by $^4\text{He}^+$ ions backscattered from lead atoms and the peak in the channel range between 80 and 120 is due to $^4\text{He}^+$ ions scattered from oxygen atoms. The oxygen peak formed at ambient air is small compared to that for the irradiated spot. The peak area of the lead peak is proportional to the number of lead atoms and the width of the peak, $HW_{\text{Pb}}^{\text{Pb}}$, is proportional to the thickness of the evaporated lead layer (l): $HW_{\text{Pb}}^{\text{Pb}} = l [S]_{\text{Pb}}^{\text{Pb}}$, where we use the subscript and

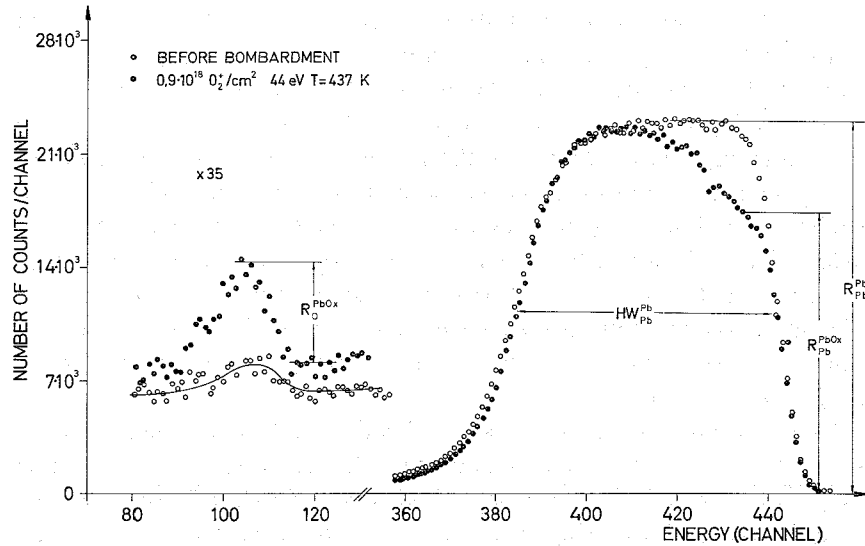


Fig. 1. Backscattering energy spectra of a lead layer before and after bombardment with $0.9 \times 10^{18} \text{ O}_2^+/\text{cm}^2$ at 44 eV and 437 K substrate temperature using 1.5 MeV $^4\text{He}^+$ -ions.

the superscript to denote the scattering atom and the medium, respectively.

The proportionality constant $[S]_{\text{Pb}}^{\text{Pb}}$ is given by⁵⁾

$$[S]_{\text{Pb}}^{\text{Pb}} = \alpha_{\text{Pb}} \left. \frac{dE}{dx} \right|_{E_0} - \frac{1}{\cos \theta} \left. \frac{dE}{dx} \right|_{\alpha_{\text{Pb}} E_0},$$

where α is the fractional amount of energy after scattering, dE/dx is the specific energy loss, and E_0 and $\alpha_{\text{Pb}} E_0$ are the energies before and after scattering at angle (θ), respectively. The height of the lead peak $R_{\text{Pb}}^{\text{Pb}}$ is given by

$$R_{\text{Pb}}^{\text{Pb}} = f N_{\text{Pb}}^{\text{Pb}} \cdot \Delta E / [S]_{\text{Pb}}^{\text{Pb}}, \quad (1)$$

where $N_{\text{Pb}}^{\text{Pb}}$ is the concentration of lead atoms in the lead layer and ΔE is the energy per channel from calibration measurements. The constant f depends on the geometry of the experimental arrangement. A similar treatment holds for the oxygen peak. A detailed description of the analysis of backscattered spectra has been given elsewhere⁸⁾. $[S]$ values for 1.5 MeV $^4\text{He}^+$ in lead and lead oxides were calculated using dE/dx values summarized by Whaling⁹⁾. For our experimental arrangement the following values are obtained:

$$\begin{aligned} [S]_{\text{Pb}}^{\text{Pb}} &= 95 \text{ eV/\AA}, & [S]_{\text{Pb}}^{\text{Pb}_2\text{O}} &= 71 \text{ eV/\AA}, & [S]_{\text{Pb}}^{\text{PbO}} &= 70 \text{ eV/\AA}, \\ [S]_{\text{O}}^{\text{Pb}_2\text{O}} &= 63 \text{ eV/\AA}, & [S]_{\text{O}}^{\text{PbO}} &= 62 \text{ eV/\AA}, \\ [S]_{\text{O}}^{\text{PbO}_x} &= 81 \text{ eV/\AA} \quad (\text{this value holds only for low O-content}), \end{aligned}$$

The last two values show that the depth scale is not constant for a tailed oxygen distribution in the oxide layer, and errors of about 25% are involved in determining the concentration profile of oxygen in the produced oxide layers.

The step in the front edge of the lead layer at the oxidized spot is mainly due to the reduced lead concentration, $N_{\text{Pb}}^{\text{PbO}_x}$, in the lead oxide. This concentration can be calculated by comparing $R_{\text{Pb}}^{\text{Pb}}$ and $R_{\text{Pb}}^{\text{PbO}_x}$, the heights of the lead peak at the surface before and after oxidation

$$\frac{N_{\text{Pb}}^{\text{PbO}_x}}{N_{\text{Pb}}^{\text{Pb}}} = \frac{R_{\text{Pb}}^{\text{PbO}_x} [S]_{\text{Pb}}^{\text{PbO}_x}}{R_{\text{Pb}}^{\text{Pb}} [S]_{\text{Pb}}^{\text{Pb}}}, \quad (2)$$

The concentration ratio of oxygen to lead atoms near the surface is given by

$$\frac{N_{\text{O}}^{\text{PbO}_x}}{N_{\text{Pb}}^{\text{PbO}_x}} = \frac{R_{\text{O}}^{\text{PbO}_x} [S]_{\text{O}}^{\text{PbO}_x} \sigma_{\text{Pb}}}{R_{\text{Pb}}^{\text{PbO}_x} [S]_{\text{Pb}}^{\text{PbO}_x} \sigma_{\text{O}}}, \quad (3)$$

where $\sigma_{\text{Pb}}/\sigma_{\text{O}} = 116$ in our experimental arrangement.

4. Results

During irradiation of lead with oxygen ions several experimental parameters are involved, such as dose rate (flux), dose (fluence), beam energy and substrate temperature. Careful experimental studies are necessary to determine the relative influence of such parameters on the results. Dose rate was kept constant at $70 \mu\text{A}/\text{cm}^2$ and no experiments have been performed on dose-rate dependence. Oxygen peaks of nonreproducible area were observed for evaporated lead layers stored in ambient air. This problem determines the choice of minimum dose ($0.9 \times 10^{18} \text{O}_2^+/\text{cm}^2$) and minimum substrate temperature (378 K) used during the course of this study. The formation of small oxide peaks before irradiation was partly avoided by storing the evaporated layers at 10^{-6} torr.

The sputtering of lead atoms by oxygen ions restricted the maximum beam energy for oxide formation to about 50 eV. For higher beam energies, irrespective of substrate-temperature sputtering without any oxide formation was observed. In fig. 2 the effect of sputtering is demonstrated in the reduction of the width of the lead peak after bombardment with $3.6 \times 10^{17} \text{O}_2^+/\text{cm}^2$ at 210 eV. The results of an analysis of such spectra produced by using different beam energies is shown in fig. 3 where the measured sputtering coefficient S is plotted versus the energy of the incident oxygen beam. The curve shows two regions typical for sputtering; slow increase in yield at low energies, followed by a steep linear increase of S at higher energies. An extrapolated threshold value of about 60 eV is obtained.

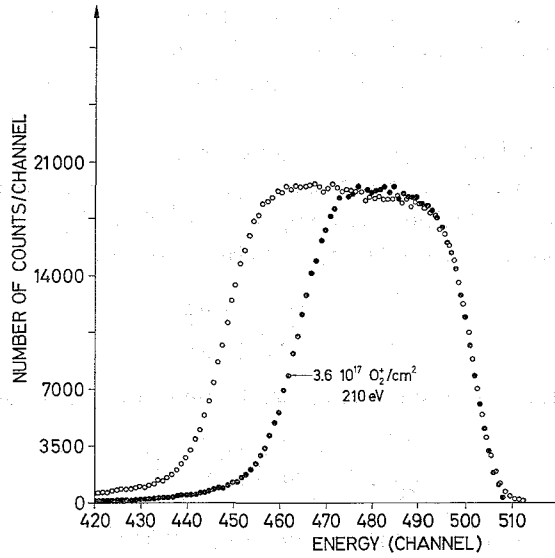


Fig. 2. Backscattering energy spectra for a lead layer before and after bombardment with $0.9 \times 10^{18} \text{ O}_2^+/\text{cm}^2$ at 210 eV and 25°C substrate temperature using 1.5 MeV $^4\text{He}^+$ -ions.

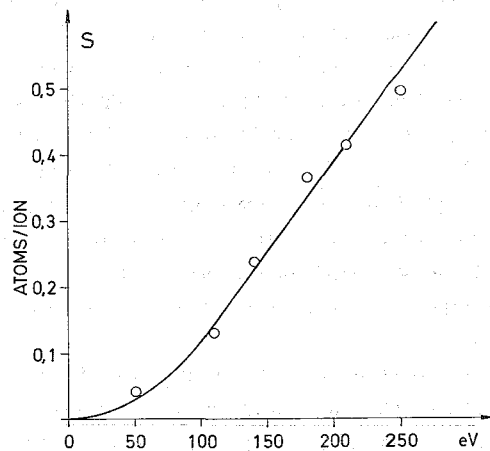


Fig. 3. Number of sputtered lead atoms per oxygen ion as a function of the energy of oxygen ions.

The substrate temperature was found to have the dominant influence on the oxide growth. This result is illustrated in fig. 4 where three oxygen peaks are shown for comparison. During irradiations both dose rate and dose were held constant; only the substrate temperature was varied. The increase of the peak area with increasing substrate temperature is mainly due to an increase

of the peak width and not to an increase in peak height, which shows the growth in thickness of oxide.

In fig. 5 the logarithm of the peak area of the oxygen peak is plotted versus the reciprocal substrate temperature. Constant dose rate of $70 \mu\text{A}/\text{cm}^2$ and constant dose of $0.9 \times 10^{18} \text{O}_2^+/\text{cm}^2$ at 44 eV were maintained during these measurements. For temperatures greater than 520 K the decomposition of the lead layer and diffusion of lead into the carbon substrate were observed. These effects determined the upper limit for the temperature range.

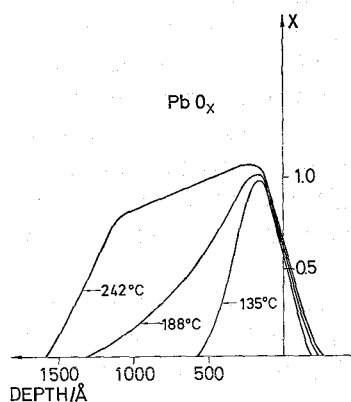


Fig. 4. Depth distribution of oxygen content x for lead samples irradiated with constant oxygen fluence at three different substrate temperatures.

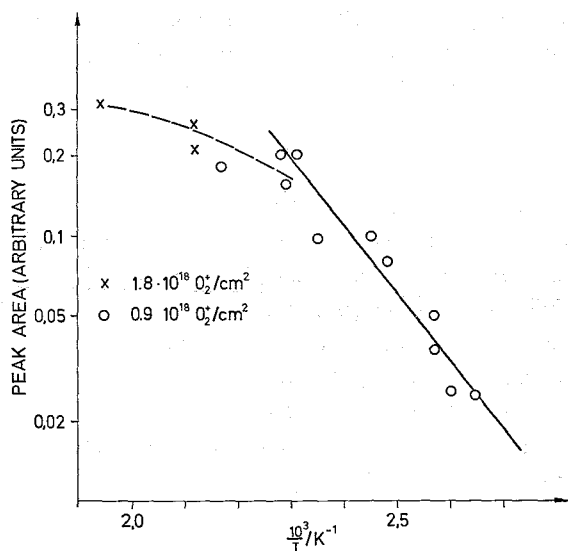


Fig. 5. Temperature dependence for ion oxidation of evaporated lead films

Having in mind that the range of 44 eV O_2^+ ions in lead is only a few Å, then the absolute thickness and the increase of thickness in fig. 4 conclusively shows that oxygen diffusion is the rate limiting mechanism in this oxidation process. The maximum peak height determines the number of lead atoms in the lead oxide. From eq. (3) the ratio of lead atoms and oxygen atoms near the surface can be obtained by measuring the height of the oxygen peak and the height of the step in the lead peak. Both the $[S]$ values for scattering from O and Pb atoms in Pb_2O and PbO were used for calculation. As a result we obtain ratios close to one in both cases. In eq. (3) the ratio of the $[S]$ values is not very sensitive to different lead-oxide compounds. Only for PbO the calculated atomic ratio does agree with the expected value for the compound. So we concluded that lead monoxide has been formed. The calculated atomic ratio is given as the ordinate in fig. 4. It should be noted that the backscattering technique does not allow to determine the crystalline forms of the same compound. Other analysis techniques have to be used. Here we use a simple chemical test and assume that orthorhombic PbO has been formed.

The nearly constant peak height at different temperatures, fig. 4, shows that the diffusion process is of the "constant source" type. In this case the total amount of diffused material is given by¹⁰⁾

$$Q = \frac{N_0}{\sqrt{\pi}} 2\sqrt{(Dt)},$$

where N_0 is the oxygen concentration near the surface, t is the oxidation time, and D is the diffusion coefficient. If D is independent of the concentration of the diffusant, then D depends only on temperature as follows:

$$D = D_0 \exp(-E/kT),$$

where E is the activation energy for the diffusion process. As t was the same in all experiments, we obtain: $Q \approx \exp(-E/2kT)$. This explains the linear increase of peak area in fig. 5 between $(2.3 \text{ and } 2.7) \times 10^{-3} \text{ K}^{-1}$. The slope of the curve gives the activation energy E . It was found to be 1 eV. For higher temperatures a saturation effect was observed. This saturation was further established by increasing the dose up to $2.5 \times 10^{18} \text{ O}_2^+/\text{cm}^2$.

A second way for determination of the activation energy is by analysing the concentration profiles of the oxygen peaks. For the case of a "constant source" the concentration profile is given by¹⁰⁾

$$N(x) = N_0 \left(1 - \operatorname{erf} \frac{x}{2\sqrt{(Dt)}} \right).$$

Then the initial slope of the profile is

$$\left. \frac{dN}{dX} \right|_{x=0} = \frac{N_0}{\sqrt{\pi}} \frac{1}{\sqrt{D}} \exp \frac{E}{2kT}.$$

This method has some disadvantage in comparison with the former method, because the initial slope is seriously affected by the detector resolution, especially in the lower temperature range, whereas the total peak area is independent of detector resolution. In addition, the slope is affected by changes in the $[S]$ value. Nevertheless, we found for E approximately the same value after a crude correction for the detector resolution had been applied.

5. Summary and discussion

Evaporated lead layers have been oxidized by bombardment with oxygen ions. Energies smaller than 50 eV were found to be necessary in order to avoid sputtering effects. The range of these ions in lead is only a few Å. As the oxide layers, made by these ions have thicknesses greater than 200 Å, diffusion is involved in the oxide formation process. It should be noted, that the energy of the O_2^+ -ions is higher than twice the dissociation energy of O_2 (18.7 eV)¹²). In the temperature range 378–473 K the oxide growth can be described by an activation energy of 1 eV. This is in agreement with earlier results presented by Hapase et al.²) for thermal oxidation in the temperature range 500–580 K.

Concerning dissociation processes of O_2 and other surface effects as possible rate limiting processes in thermal oxidation, Hapase et al. have found a parabolic time dependence for the oxidation process. This result determines diffusion as the rate limiting process. As our activation energy agrees with that found by Hapase et al., we assume that the same diffusion limited oxidation process is involved. This assumption is further justified by the direct observation of the diffusion profiles shown by the oxygen peaks in our spectra. The evaluated activation energy for diffusion determined from these profiles was the same as the activation energy for oxidation determined from the area of the oxygen peak. This conclusively shows that the diffusion process is the rate limiting process for forming thick oxide layers. The processes of forming the diffusant (e.g., dissociation of O_2) are fast processes. It should be mentioned that Thompson and Strong¹¹) found an activation energy for diffusion of 1 eV for diffusion of oxygen through PbO.

In our oxide layers the ratio of oxygen to lead atoms was found to be 1 near the surface. Andersson and Tare¹) studied the structure of lead oxide layers by RHEED techniques and determined that orthorhombic lead monoxide

was formed during thermal oxidation. This is in agreement with our conclusion that lead monoxide has been formed.

References

- 1) J. R. Anderson and V. B. Tare, *J. Phys. Chem.* **68** (1964) 1482.
- 2) M. G. Hapase, M. K. Gharpurey and A. B. Biswas, *Surface Sci.* **12** (1968) 85.
- 3) J. H. Freeman et al., in: *European Conference on Ion Implantation*, Reading (1970).
- 4) M. Watanake and A. Tooi, *Japan. J. Appl. Phys.* **5** (1966) 737.
- 5) O. Meyer, J. Gyulai and J. W. Mayer, *Surface Sci.* **22** (1970) 263.
- 6) O. Meyer and W. Scherber, *J. Phys. Chem. Solids* **32** (1971) 1909.
- 7) A. Hiraki, M. A. Nicolet and J. W. Mayer, *Appl. Phys. Letters* **18** (1971) 178.
- 8) J. W. Mayer, L. Eriksson and J. A. Davies, *Ion Implantation in Semiconductors* (Academic Press, 1970).
- 9) W. Whaling, in: *Handbuch der Physik*, Band 34, Ed. S. Flügge (Springer, Berlin, 1958) p. 193.
- 10) B. J. Boltaks, *Diffusion in Semiconductors* (Infosearch, London, 1963) p. 104.
- 11) B. A. Thompson and R. L. Strong, *J. Phys. Chem.* **67** (1963) 594.
- 12) M. von Ardenne, *Tabellen zur Angewandten Physik*, Bd. I (Berlin, 1962) p.585.

DIFFUSION PROCESSES AT THE Cu-CdTe INTERFACE FOR EVAPORATED AND CHEMICALLY PLATED Cu LAYERS

H. Mann,* G. Linker and O. Meyer

Institut für Angewandte Kernphysik, Kernforschungszentrum Karlsruhe, Germany

(Received 24 May 1972 by E.F. Bertaut)

Diffusion of Cu into CdTe was studied at temperatures over the range 290–350°C by use of $^4\text{He}^+$ ion backscattering. Cu diffusion from an evaporated Cu layer on CdTe is found to be lower, by a factor of 10^4 , than previously reported results for diffusion of Cu from a Cu_2Te layer on CdTe. Enhanced penetration of Cu is also observed to occur during chemical plating at lower temperatures (i.e. $<100^\circ\text{C}$).

DIFFUSION processes are important in formation of metal electrodes and compounds in surface layers of crystals. Cu_{2-x}Te layers on CdTe crystals, in particular, are of interest for electro-optic applications of this material.¹ The non-destructive character of the nuclear backscattering technique, and the sensitivity in terms of mass and thickness resolution of surface layers, make it well suited to such investigations of metal electrodes on crystalline substrates.² In the present work the backscattering technique is shown to be applicable to simultaneous measurement of compound formation and diffusion for Cu in CdTe.

Previous studies of diffusion by use of backscattering³ are for low concentrations (i.e. <1 at.%) of foreign atoms. In that case the effect of the diffusant on the specific energy loss dE/dx in the material is negligible. In the present work we are concerned with determination of diffusion parameters when dE/dx in the substrate is expected to have undergone a significant change due to a higher concentration of diffusing atoms. The effect of concentration on dE/dx can be obtained from data given by Whaling.⁴

Cu layers were evaporated onto freshly etched CdTe single crystals, and CdTe layers were evaporated onto polished graphite substrates. Chemical plating of Cu onto the crystals and the evaporated layers was performed at temperatures from 3 to 85°C. Backscattering of 2.0 and 2.8 MeV $^4\text{He}^+$ ions was used for recording diffused impurity profiles as described in earlier work.⁵ Diffusion was performed in 10 or 20 min intervals at 290, 320 and 350°C in an N_2 atmosphere.

The measurement is illustrated in Fig. 1 for the case of an evaporated Cu layer on a CdTe crystal. Before heat treatment the initial thickness of the Cu layer is represented on the energy scale as the interval from 1.58 MeV (leading edge), corresponding to backscattering from Cu atoms at the surface, down to 1.33 MeV (trailing edge) for backscattering from Cu atoms at the Cu-CdTe interface. The Cu layer is sufficiently thick that the leading edge for backscattering from the CdTe crystal is shifted below the leading edge for Cu and is seen at 1.48 MeV. During successive heat treatments the thickness of the Cu layer decreases, causing the leading edge for CdTe and the trailing edge for Cu to move towards higher energy. In Fig. 1 it is also shown that, for the prolonged heat treatment used, Cd moves through Cu and appears at the surface of the Cu layer. This process was

* On leave of absence from Argonne National Laboratory, Argonne, Illinois 60439.

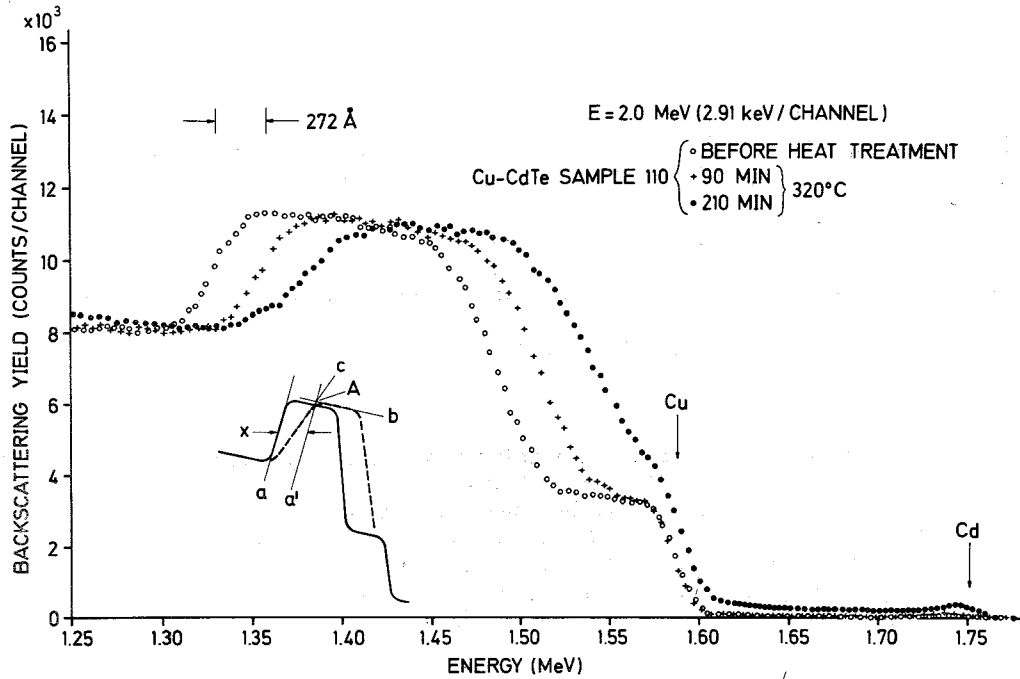


FIG. 1. Experimental spectra illustrating the shift of the leading edge for CdTe (initially 1.48 MeV) and the trailing edge for Cu (initially 1.33 MeV) during diffusion of Cu from an evaporated layer into a CdTe crystal. The graphical method for construction of the Cu-CdTe (Cu) interface after diffusion is shown in the inset.

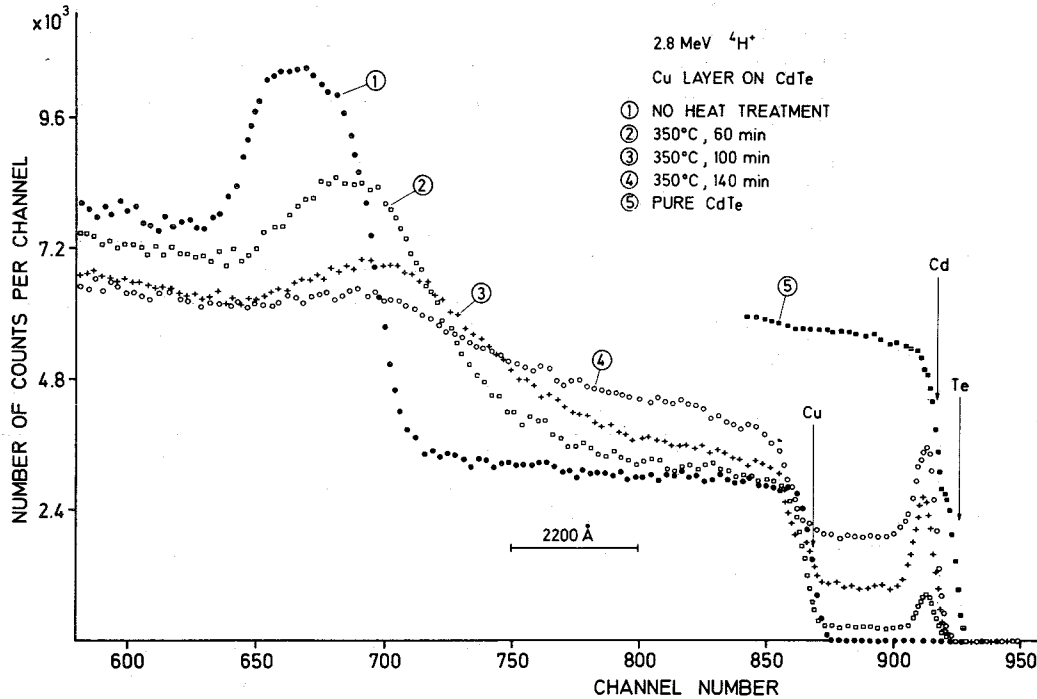


FIG. 2. Experimental spectra illustrating outdiffusion through an evaporated layer of Cu on a CdTe crystal. By comparison with the spectrum (■) for a CdTe crystal without a Cu layer it is clearly seen that Cd outdiffusion has occurred.

studied in detail and is illustrated in Fig. 2. A barrier in the form of an oxide or thin evaporated Al layer, was necessary in order to record the amount of Cd that has diffused through the Cu layer. First, the Cd diffuses rapidly through Cu and sticks at the Cu surface when there is a barrier. Then, after prolonged heat treatment, Cd is found to be uniformly distributed throughout the Cu.

The recorded diffused impurity profile (trailing edge) of the Cu layer in Fig. 1 is dependent on the real diffusion profile and the backscattering energy loss parameter $[S]$.⁶ $[S]$ is a function of the composition and remains an unknown quantity. Also, the diffusion may be enhanced in the vicinity of grain boundaries, possibly affecting the diffused impurity profile.⁷ In order to overcome these effects we use a simple graphical analysis method to determine the thickness of the Cu layer after each heat treatment. The graphical analysis method shown in the inset of Fig. 1 is used to obtain the new location of the interface; portions of the spectra may be approximated by straight lines. The location of the interface at $t = 0$ is given by line a. The new interface after heat treatment is line a' through point A and parallel to line a. The point A, found by the intersection of lines b and c, represents the lowest energy for backscattering from a layer containing 100 at.% Cu. The horizontal distance x between a and a' is proportional to the quantity Q of Cu that has diffused into CdTe. Because dE/dx for $^4\text{He}^+$ in Cu is known we can convert the energy scale to a depth scale⁴ by $d(\text{\AA}) = x(\text{keV})/[S]$.

The diffusion problem of Cu in CdTe is that for a constant source, and is described by⁸

$$Q = \frac{2N_0}{\sqrt{\pi}} \cdot \sqrt{Dt} \text{ or } d = \frac{2}{\sqrt{\pi}} \cdot \sqrt{Dt}$$

where N_0 = concentration of Cu atoms ($8.5 \times 10^{22} \text{ cm}^{-3}$) in the Cu layer, Q = number of Cu atoms per cm^2 leaving the Cu layer at time t by diffusion and t = time in sec.

Figure 3 shows the results of measurements of x for evaporated Cu layers on CdTe after diffusion at three different temperatures. The diffusion coefficients D obtained from these measurements can be described by an Arrhenius equation

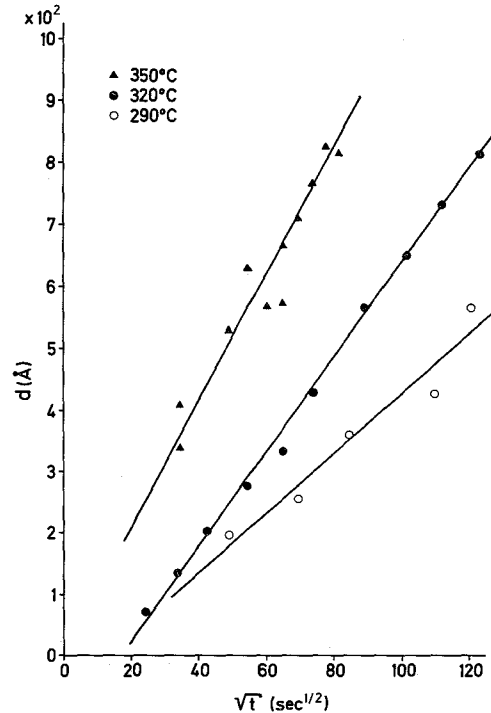


FIG. 3. Observed decrease d in the thickness of the Cu layer on CdTe during diffusion at 290, 320 and 350°C. From these data the diffusion coefficient D is found to be $(1.88, 4.71 \text{ and } 8.56) \times 10^{-15} \text{ cm}^2 \text{ sec}^{-1}$ at 290, 320 and 350°C, respectively. Values for d are obtained from the measured values for x according to $d(\text{\AA}) = x(\text{keV})/[S]$.

$$D = D_0 \exp. (-E/kT)$$

where $D_0 = (8.2 \pm 0.8) \times 10^{-8}$ and $E = 0.64 \pm 0.04 \text{ eV}$. It is interesting to compare these results with the values $D_0 = 3.7 \times 10^{-4}$ and $E = 0.67 \text{ eV}$ obtained by Woodbury and Aven⁹ in studies of diffusion of Cu into CdTe from a Cu_2Te layer. We obtain the same activation energy, but D_0 is 4 orders of magnitude lower for diffusion from evaporated Cu layers as compared with diffusion from the compound. Thus, the surface of the CdTe strongly influences D_0 , and it is possible that surface related effects can be used to increase or decrease this quantity.

For further confirmation of this observation we evaporated layers of CdTe onto polished graphite substrates and performed chemical plating of Cu with and without formation of the Cu_2Te compound. In both cases Cu is observed to have penetrated through the CdTe layer during plating

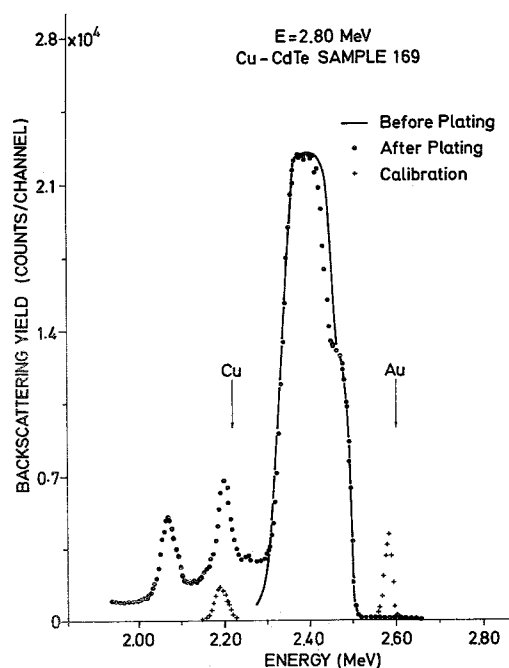


FIG. 4. Typical experimental spectra illustrating a thin (1500 Å) CdTe layer (—) before and (●) after chemical plating for 3 min at 85°C. After plating a step is produced in the CdTe leading edge as a result of formation of Cu_2Te . Below the CdTe trailing edge there are two peaks; one at 2.20 MeV due to Cu in Cu_2Te and another at lower energy due to Cu that has penetrated through CdTe to the graphite substrate. Calibration peaks (+) for Cu and Au were obtained by use of a thin layer of these elements on graphite.

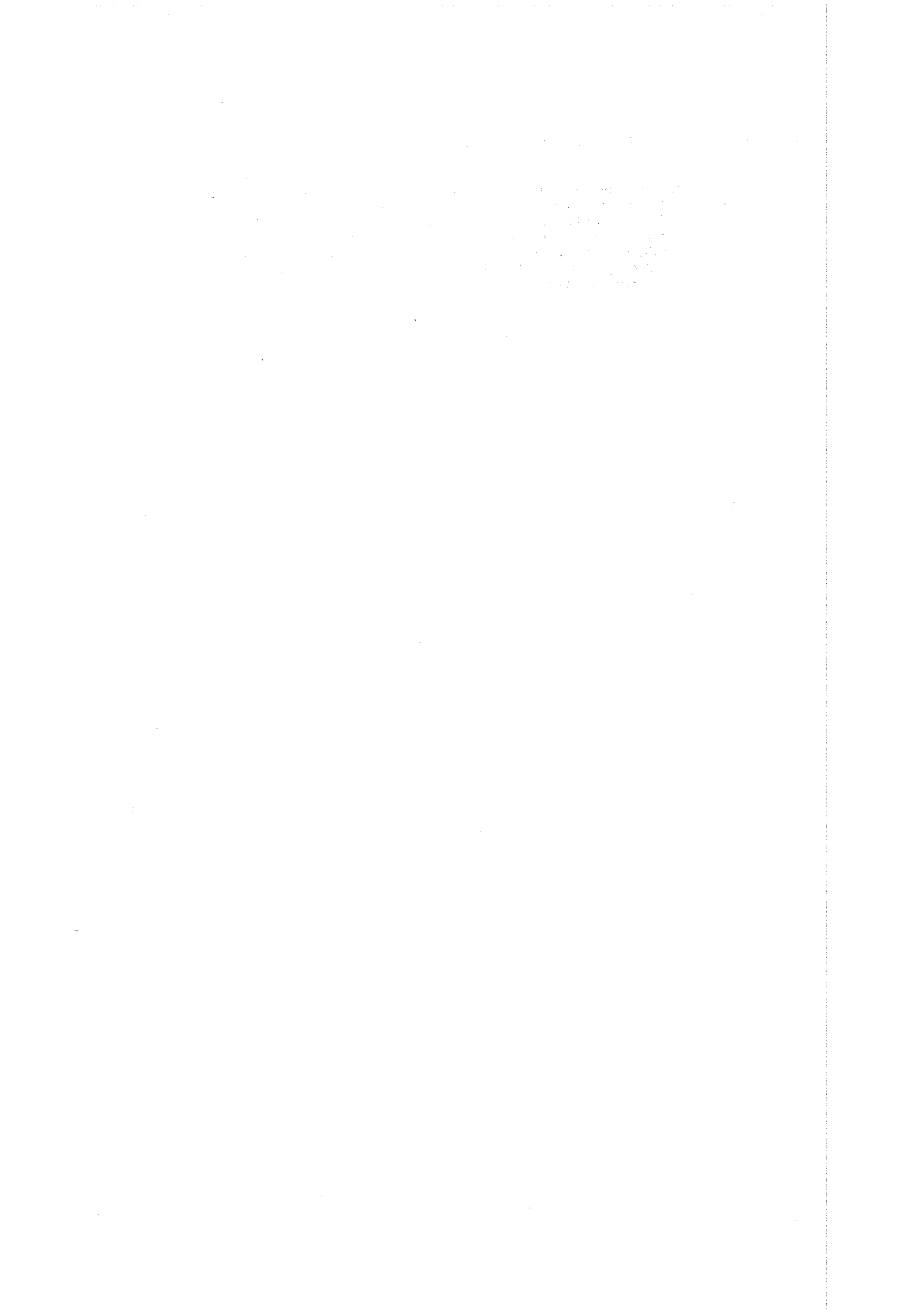
at extremely low values of time (i.e. 1–10 min) and temperature (i.e. 3–90°C), in contrast with the longer time (i.e. 10 min–2 hr) and higher temperature (i.e. 290–350°C) required for comparable diffusion from an evaporated layer. As an example, we show in Fig. 4 the energy spectra for a thin (1500 Å) CdTe layer before and after chemical plating according to the method used by Woodbury and Aven⁹ in formation of the Cu_2Te compound. The step at higher energy shows that the compound has formed. Cu in the compound is revealed at the energy of 2.20 MeV. The peak at lower energy is due to Cu that has penetrated through the CdTe layer to the graphite substrate. From such spectra we can determine the thickness of the Cu_2Te layer, the quantity of Cu in the compound, and the quantity of Cu that has diffused or penetrated either from the compound or from the solution.

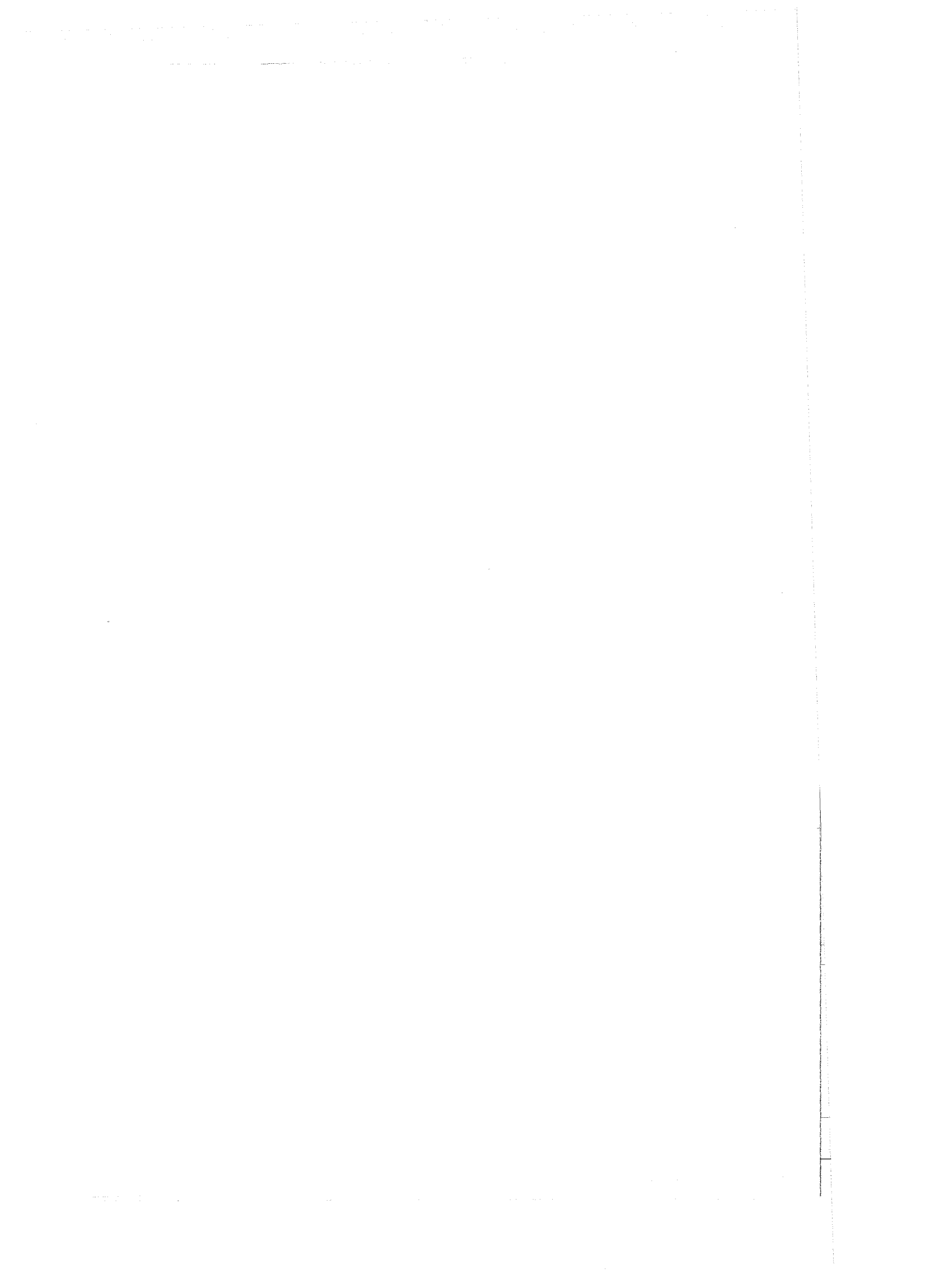
Additional studies are underway in order to obtain quantitative information, by use of backscattering, on the formation of the Cu_2Te compound and the role of the surface in enhancement of Cu penetration into CdTe.

REFERENCES

1. CUSANO D.A., *Solid State Electron.* **6**, 217 (1963).
2. HIRAKI A., LUGGUJO E., NICOLET M.-A. and MAYER J.W., *Phys. Status Solidi (a)* **7**, 401 (1971).
3. MEYER O. and MAYER J.W., *J. appl. Phys.* **41**, 4166 (1963).
4. WHALING W., *Handbuch der Physik XXXIV*, p. 193–217, edited by FLÜGGE S. (1958).
5. MEYER O., GYULAI J. and MAYER J.W., *Surface Sci.* **22**, 263 (1970).
6. MITCHELL I.V., KAMISHIDA M. and MAYER J.W., *J. appl. Phys.* **42**, 4378 (1971).
7. MEYER O., MANN H. and LINKER G., *Appl. Phys. Lett.* **20**, 259 (1972).
8. BOLTAKS B.I., *Diffusion in Semiconductors*, Infosearch, London (1963).
9. WOODBURY H.H. and AVEN M., *J. appl. Phys.* **39**, 5485 (1968).

Die Diffusion von Cu in CdTe wurde im Temperaturbereich 290–350°C mit Hilfe der Rückstreuung von $^4\text{He}^+$ -Ionen untersucht. Es wird gefunden, daß die Cu-Diffusion von Cu-aufgedampften Schichten auf CdTe um einen Faktor von 10^4 geringer ist, verglichen mit früheren Ergebnissen für die Cu-Diffusion von Cu_2Te -Schichten auf CdTe. Eine verstärkte Wanderung von Cu durch CdTe wird beim chemischen Plattieren bei niedrigeren Temperaturen (d.h. $< 100^\circ\text{C}$) beobachtet.





phys. stat. sol. (a) 14, 605 (1972)

Subject classification: 3 and 11; 1.5; 22.6

Institut für Angewandte Kernphysik, Kernforschungszentrum Karlsruhe

Impurity Incorporation during rf Sputtering of Silicon Oxide Layers

By

S. PETERSSON¹), G. LINKER, and O. MEYER

Backscattering and channeling effect measurements have been used to analyse silica rf sputtered in argon atmosphere. Layers sputtered from fused quartz were found to be stoichiometric SiO_2 irrespective of variations of sputtering parameters during film growth. Variation of power density (deposition rate) does not influence the Ar content. The amount of Ar increases with increasing bias voltage. The lowest Ar content (0.4 mol%) was found at zero bias voltage. Traces of backing material used to establish good heat transfer between substrate and anode plate have been incorporated during film growth. The amount of impurities increased with increasing bias voltage. Contrary to Ar incorporation it has been observed that the In content decreased with increasing deposition rate.

Rückstreu- und Channelingmessungen wurden für die Analyse von in Argonatmosphäre HF-gesputtertem Siliziumoxid benutzt. Schichten, die von reinem Quarz gesputtert wurden, erwiesen sich als stöchiometrisches SiO_2 , unabhängig von Änderungen der Sputteringparameter während des Schichtwachstums. Änderung der Leistungsdichte (Aufdampftrate) beeinflusst den Ar-Gehalt nicht. Der Anteil von Ar nimmt mit steigender Vorspannung zu. Der niedrigste Ar-Anteil (0,4 Mol%) wird ohne Vorspannung gefunden. Spuren des Trägermaterials, das für einen guten Wärmeübergang zwischen Substrat und Anode benutzt wurde, wurden während des Schichtwachstums eingebaut. Der Anteil der Verunreinigungen nahm mit steigender Vorspannung zu. Im Gegensatz zum Ar-Einbau wurde beobachtet, daß der In-Anteil mit steigender Aufdampftrate abnimmt.

1. Introduction

Physical properties of sputtered layers are affected by gaseous and other impurities incorporated during the sputtering process. Numerous work has been done to study the argon and nitrogen concentration in layers deposited by different sputtering techniques as a function of gas pressure, power density, bias voltage, and substrate temperature [1 to 4]. Besides the carrier gas necessary to maintain the plasma, other impurities may be accidentally incorporated. These can come from bonding and backing materials, incomplete rf shielding or the incomplete coverage of the electrodes with target and substrate materials. It is obvious that impurities in the argon gas and in the target material should also be found in the sputtered layers. The incorporated impurity concentrations similar to the argon content will also depend on sputtering parameters. Various techniques have been used to study gas entrapment in sputtered layers. The X-ray fluorescence technique was used to determine the Ar content of rf sputtered SiO_2 films as a function of film thickness, rf power density, and substrate

¹) Short-term visitor from Electronics Department, Institute of Technology, University of Uppsala.

temperature [3]. Further, laser degassing or flash heating techniques followed by a mass spectrometer analysis were used to determine Ar concentration in sputtered tantalum [1], tungsten [4], and nickel [2] films. Another suitable method of analysing films having thicknesses in the range of 500 to 5000 Å, is the backscattering and channeling technique using light ions of MeV energies. With this nondestructive technique, concentrations and depth distributions of all components of the thin film can be determined. The method has already been successfully applied to the analysis of dielectric layers, for example thermally grown SiO₂ layers [5] and Si₃N₄ layers deposited in a glow discharge [6]. In the present investigation, silicon oxide layers sputtered on single crystal Si substrates have been investigated in terms of stoichiometry, impurity content and influence of sputter etching on the substrate.

2. Experimental

The silicon oxide layers were sputtered on single-crystal silicon cut normally to the $\langle 111 \rangle$ direction. Prior to deposition the surfaces were mechanically polished and chemically cleaned using standard methods. In addition some samples were sputter etched for surface cleaning. Samples were mounted on a silicon oxide coated holder, the SiO₂ being used to prevent sputtering of substrate electrode material. For good thermal contact the samples were bonded to the substrate holder with a standard Ga-In-Sn eutectic. A 5 inch diameter fused quartz plate was used as a target material.

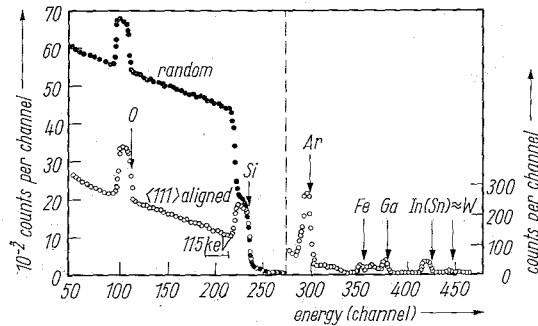
Substrate and target holders were water cooled with the target to substrate distance being kept constant at 7.2 cm during the sputtering process. A background pressure of 5×10^{-7} Torr was achieved. The purity of the argon was 99.9995% and a pressure of 5×10^{-3} Torr was usually maintained during sputtering. Prior to deposition the SiO₂ target was presputtered onto a removable shield, for 5 min. At zero bias and a rf power density of 2 Wcm⁻², the deposition rate was 100 Å/min. Thicknesses of most of the sputtered layers were in the range of 1200 to 1500 Å.

Backscattering and channeling effect measurements were performed using a beam of 2.8 MeV ⁴He⁺ ions. The samples were mounted on a 2-axis goniometer for substrate alignment. Beam currents were measured with a current integrator and secondary electrons were suppressed. Particles backscattered through a laboratory angle of 168° were detected in a surface barrier detector and the system resolution was 16 keV. Detector signals were amplified and then stored in a multichannel analyzer. The energy to channel number conversion, which was calculated from the spectrum of a C-Al-Cu-Au calibration sample, was 4.5 keV per channel. Beam currents used were from 15 to 20 nA.

3. Analysis

In Fig. 1 a typical spectrum of a silicon oxide layer sputtered on a single crystal silicon substrate is shown. From well known collision kinetics and the experimental geometry, the energy scale can be converted to a mass scale. The energies of ⁴He⁺ ions backscattered from atoms of different masses at the surface of the silicon oxide layer are well resolved in the energy spectrum, and the corresponding masses are indicated in the figure. By alignment of the incoming beam direction with the $\langle 111 \rangle$ axis of the silicon substrate, the number of back-

Fig. 1. Random and $\langle 111 \rangle$ aligned spectra for 2.8 MeV $^4\text{He}^+$ ions scattered from a silicon oxide layer deposited on $\langle 111 \rangle$ -oriented silicon by rf sputtering (300 W, 80 V bias). The right-hand scale refers to the part of the spectrum right of the vertical dashed line



scattered particles from the substrate atoms is reduced. This alignment leads to an improved analysis of the silicon oxide layer. Normalization of the random spectrum to the aligned silicon substrate level, allows separation of $^4\text{He}^+$ particles backscattered from silicon atoms in the oxide layer and in the substrate close to the interface. With this procedure [7] the peak area for silicon in the oxide layer can be determined. This is important, as peak areas in the spectra are proportional to the total amount of atoms in a layer. For a Mass M :

$$A_M = f \sigma_M N_M \Phi \quad (1)$$

with A_M peak area, σ_M Rutherford scattering cross section, N_M total number atoms, Φ total incoming flux, f proportionality factor for the geometrical arrangement.

For a homogeneous distribution of atoms in a layer, the concentration ratio for two different masses M_1 and M_2 can be determined from equation (1):

$$\frac{N_{M_1}}{N_{M_2}} = \frac{A_{M_1} \sigma_{M_2}}{A_{M_2} \sigma_{M_1}} \quad (2)$$

If an absolute concentration is known (for example for the Si atoms in the substrate layer) other absolute concentrations can be calculated by equation (2). The energy scale in Fig. 1 can be converted to a depth scale if the specific energy loss is known. The energy resolution of the detecting system determines the ultimate depth resolution. Depending on the incident particle energy, the depth resolution is found to be in the range of 200 Å; within this accuracy depth profiles can be determined. A more detailed treatment of the analysis problems is given by Meyer et al. [5].

4. Results

The ratio of oxygen to silicon atoms, from [2], obtained by the analysis of 25 oxide layers sputtered from fused quartz, is found to be 2.05 ± 0.1 . From this result it is concluded that stoichiometric amounts of each component has been sputtered and deposited during film growth. Over the ranges of power density and bias voltages used, no change in this stoichiometry was observed.

Sputter etching for 5 min at 400 W prior to deposition produces heavy radiation damage at the surface of a single crystal Si substrate. This is clearly seen in the $\langle 111 \rangle$ -aligned spectrum in Fig. 2. A sharp peak is visible at the interface

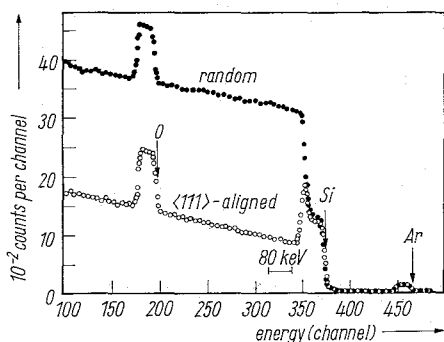


Fig. 2. Random and $\langle 111 \rangle$ -aligned spectra for 2.8 MeV $^4\text{He}^+$ ions scattered from a silicon oxide layer deposited by rf sputtering (400 W, zero bias). The substrate was sputter etched prior to deposition

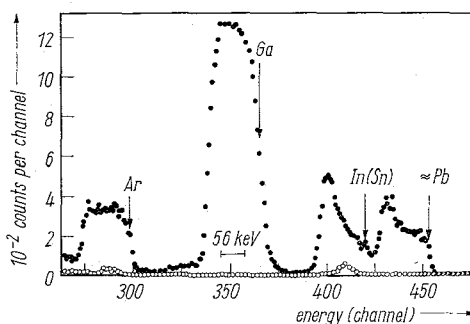


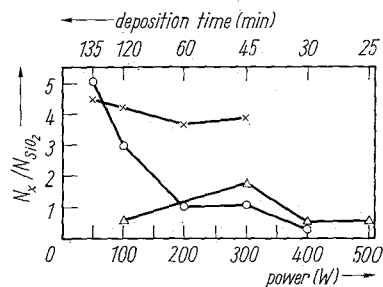
Fig. 3. Backscattered impurity spectra for 2.8 MeV $^4\text{He}^+$ of sputtered layers showing extremely high impurity content (closed circles) and reasonable low impurity content (open circles). ●: 170 V; 300 W, ○: 0 V; 100 W

between Si and SiO_2 . This peak is due to scattering from disordered Si atoms at the substrate surface. The thickness of the damaged layer is estimated to be 300 to 400 Å, which is in agreement with results published by Davidson [8]. Far less disorder is detected when Si surfaces are chemically etched. A disordered layer can cause problems because the main assumption in the analysis is the existence of a sharp interface between the substrate and the sputtered layer. The plateau of the Ar peak indicates that Ar is equally distributed throughout the thickness of the deposited layer (see Fig. 2).

The impurity content in the oxide layer was found to be strongly dependent on the sputtering conditions. The large effect of bias sputtering on the impurity concentration is demonstrated in Fig. 3, where the high energy parts of two spectra are shown for comparison. At zero bias voltage, the oxide layer is rather clean and the impurity level is below 10 ppm in average. About 0.4% Ar are found in this layer. In contrast a 5000 Å thick oxide layer, produced with 15% bias (170 V), exhibits at least 4 big impurity peaks. Besides Ar, In and/or Sn (mass resolution in this mass range does not allow separation), a heavy mass with a mass number of about 200 ± 10 can be detected. These materials probably stem from the backing material that was used to obtain good heat conductivity between substrate and target electrode. It is assumed that during the sputtering process part of this material becomes gaseous, due to substrate heating and/or bias sputtering. The rectangular shape of the Ar peak indicates that the Ar is equally distributed throughout the SiO_2 layer, the same situation also occurs for the Ga peak. The In peak and the high mass peak however, show a marked decrease in concentration towards the surface of the oxide layer. This decrease of impurity concentration may be explained by either a drop in vapor pressure during film growth or by outdiffusion of impurities. This outdiffusion can occur because of enhanced layer heating during prolonged deposition times for bias sputtering.

In an initial experiment the depositions were performed using various power densities and the influence of deposition rate on impurity content was studied. By increasing the power density, to keep layer thicknesses to about 1200 Å, deposition times were reduced from 135 to 25 min. At 6% bias voltage the

Fig. 4. Impurity content versus power density with bias voltage as a parameter. \times : Δ Ar (0% bias); \times Ar (6% bias); \circ In (6% bias)



absolute bias voltage increases from 30 to 100 V, with increasing power density.

The results of these initial experiments are summarized in Fig. 4. The Ar content versus power density is shown for two sets of samples produced with zero and 6% bias voltage. In both cases only a little dependence of Ar concentration on power density is found but there is a marked difference in absolute values. This independence of Ar content on rf power density was also found by Hoffmeister and Zuegel [3].

For zero bias voltage, the Ar content was found to have values between 0.4 and 1.8 mol% (compared to the number of SiO_2 molecules in the oxide layer). The Ar concentration from 75% of the measured layers was found to be 0.4, 0.5, and 0.6 mol% so it is assumed that the value of 1.8% at 300 W power is exceptionally high. At 6% bias voltage, the Ar concentration slowly decreases with increasing power from 4.5 to 3.7 mol%. The only other pronounced impurity peak found in these samples was attributed to scattering from In(Sn) atoms. The In(Sn) content decreases with increasing power or decreasing deposition time. This result indicates that the process of entrapment is different for In(Sn) and Ar. The deposition rate of sputtered target atoms is found to be inversely proportional to the deposition rate of In and proportional to the deposition rate of Ar atoms.

A further experiment was to investigate the dependence of the impurity content on bias voltage, the results are shown in Fig. 5. A constant power density of $2 W cm^{-2}$ was used during sputtering. Equal layer thicknesses of about 1200 Å were obtained by increasing the deposition time with increasing bias voltage. The lowest Ar content was found at the zero bias voltage with steep increase of Ar content, occurring when the bias voltage is applied. To verify this the results discussed above are included (dashed curve). With in-

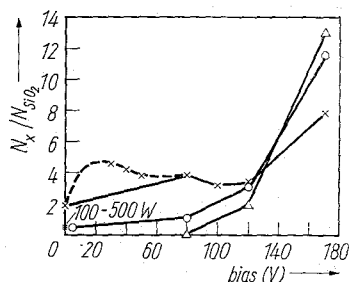


Fig. 5. Impurity content versus bias voltage at 300 W power. \times : Ar (data in %); \circ In (‰); Δ Ga (‰)

creasing bias voltage up to 120 V, the Ar content decreases slightly from 4.5 to 3.1 mol%. For voltages greater than 120 V, a steep increase of Ar concentration is found. This steep increase may be due to an enhanced sticking probability for Ar ions with energies above 120 eV in the SiO₂ substrate.

Altering the bias voltage also appeared to change the concentration of Ga. A similar dependence to that of Ar with bias voltage was observed for the Ga and In(Sn) contents in the sputtered layer. The amount of Ga and In(Sn) increases strongly with increasing bias voltage (note the different scale factors); the same increase was also obtained for the high-mass impurity peak. An increase of the Fe content in sputtered SiO₂ layers on Si substrates with increasing bias voltage, was also found during bias sputtering when substrate holders were incompletely coated. It can be concluded from these results that bias sputtering, with bias voltages of about 100 V or above, will generally lead to an enhanced incorporation of impurities in the layer. For the layer with extremely high impurity content anneal experiments were performed. After 30 min anneal at 600 °C and 10⁻⁷ Torr, the Ar content dropped from 8 to 3 mol%. Further isochronal anneal treatments at 600 °C and 700 °C did not noticeably change the Ar concentration. This is in contrast to results presented by Hoffmeister and Zuegel [3] who found that almost all of the Ar was lost within a one hour anneal at 600 °C. The heavy mass impurity and the In(Sn) content was not affected by this anneal treatment. This indicates that the depth distributions of these impurities are probably due to a decrease of vapor pressure during deposition. A 30% decrease of Ga content was found however during heat treatment.

5. Discussions and Conclusions

The impurity content of silica layers, deposited by bombarding a fused quartz target with Ar ions generated in a rf glow discharge, was determined by means of backscattering and channeling effect measurements. The oxide layers were found to be stoichiometric SiO₂ irrespective of various sputtering parameters used during film growth. This result is in contrast to results obtained by the analysis of reactively sputtered silica layers [9]. Here it was found that the ratio of oxygen to silicon atoms strongly depends on the oxygen gas pressure. It was observed that sputter etching of the Si substrate prior to film deposition, caused severe damage at the substrate surface. This damage may cause electrical irregularities at the interface Si/SiO₂ and should be avoided.

At zero bias voltage, the Ar concentration was found to be in the range of 0.5 to 1.8 mol%. This is in agreement with results given by Hoffmeister and Zuegel [3] for rf sputtered SiO₂ layers. Applying small rf bias voltages to the substrate results in an increase of Ar content to about 4 mol%. This increase may be related to the absorption of low-energy Ar ions originated in the glow discharge, a mechanism which has been discussed by Lee and Oblas [4]. After increasing the bias voltage above 120 V a further increase of Ar content is observed. The absorption mechanism responsible for this enhanced increase may be due to entrapment of energetic neutral Ar atoms as discussed by Winter and Kay [2]. Rf power density variation showed only a little influence on Ar content. In all cases the entrapped Ar was found to be equally distributed throughout the layer thickness. Substrate holder material and backing material was found to be incorporated during the rf bias sputtering process. A minimum impurity concentration was found for layers produced at zero bias voltage.

It was found that the impurity concentration strongly increased for bias voltages above 120 V. In contrast to Ar, the number of In atoms trapped in the films decreased with increasing power. To summarise, we conclude that biased rf sputtering does not have any advantages in the production of pure SiO₂ films. If other properties, such as the enhanced mechanical strength are improved by bias sputtering, then moderate bias voltages (below 120 V) may be tolerated.

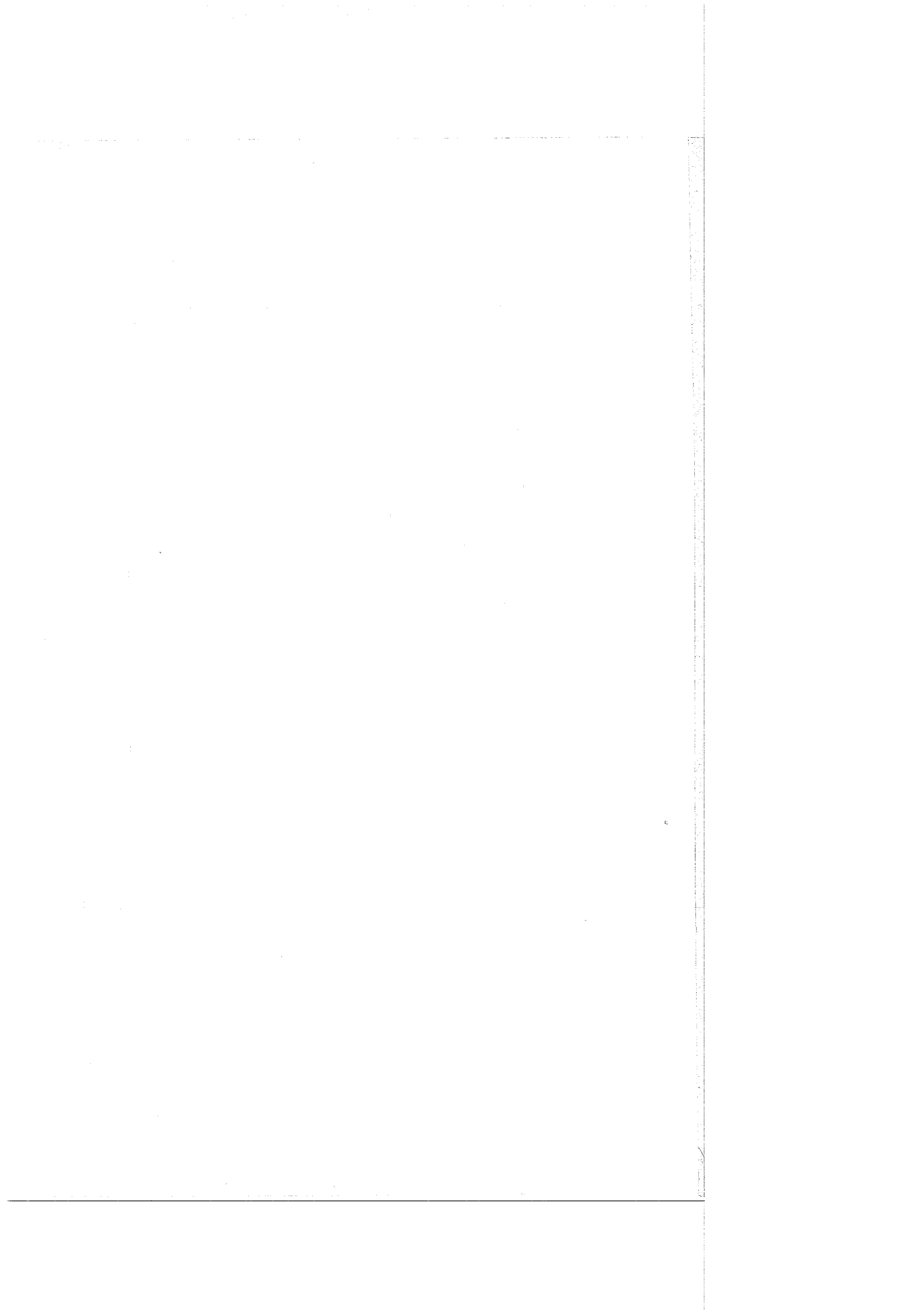
Acknowledgements

We gratefully acknowledge the assistance of Mr. A. Hyder who planned and performed the sputtering experiments. We also wish to thank Dr. M. Gettings and Prof. P. A. Tove for valuable discussions.

References

- [1] D. GERSTENBERG and C. J. CALBICK, *J. appl. Phys.* **35**, 402 (1964).
- [2] H. F. WINTERS and E. KAY, *J. appl. Phys.* **38**, 3928 (1967).
- [3] W. HOFFMEISTER and M. ZUEGEL, *Thin Solid Films* **3**, 35 (1969).
- [4] W. W. LEE and D. OBLAS, *J. Vacuum Sc. and Technol.* **7**, 129 (1970).
- [5] O. MEYER, J. GYULAI, and J. W. MAYER, *Surface Sci.* **22**, 263 (1970).
- [6] O. MEYER and W. SCHERBER, *J. Phys. Chem. Solids* **32**, 1909 (1971).
- [7] M. KAMOSHIDA, I. U. MITCHELL, and J. W. MAYER, *Appl. Phys. Letters* **18**, 292 (1971).
- [8] S. M. DAVIDSON, *J. Mater. Sci.* **7**, 473 (1972).
- [9] G. LINKER and O. MEYER, unpublished results.

(Received July 26, 1972)



phys. stat. sol. (a) **16**, 377 (1973)

Subject classification: 2; 22.S.1

*Institut für Angewandte Kernphysik, Kernforschungszentrum Karlsruhe (a)
and AEG-Telefunken, Heilbronn (b)*

Analysis of Phosphosilicate Glass Layers by Backscattering and Channeling Effect Measurements

By

G. LINKER (a), O. MEYER (a), and W. SCHERBER (b)¹⁾

Rutherford backscattering and channeling effect measurements are used to study the composition of phosphosilicate glass (PSG) layers in the system PSG-SiO₂-Si. Using an incident beam of 2.8 MeV ⁴He⁺ ions, backscattered particles from P atoms could be well separated from those scattered from Si isotopes in the energy spectra. Phosphorus concentration and phosphorus behaviour during anneal treatment was determined from P-peak analysis. Concerning the absolute values no agreement with the existing phase diagram of the system SiO₂-P₂O₅ could be established. A scattering cross section enlargement of about 20% for oxygen was observed with 2.8 MeV helium ions.

Rückstreu- und Channelingeffektmessungen wurden zur Untersuchung der Zusammensetzung von Phosphosilikatglasschichten (PSG) im System PSG-SiO₂-Si durchgeführt. Durch Verwendung einer Primärenergie von 2,8 MeV konnten die von den P-Atomen und den Si-Isotopen rückgestreuten ⁴He⁺-Ionen im Energiespektrum gut voneinander getrennt werden. Die Phosphorkonzentration und das Verhalten des Phosphors während einer Temperaturbehandlung wurde durch Analyse des P-Peaks bestimmt. Eine Übereinstimmung der absoluten Konzentrationen mit dem bestehenden Phasendiagramm für das System SiO₂-P₂O₅ konnte nicht erzielt werden. Eine Vergrößerung des Streuquerschnitts von etwa 20% für die Sauerstoffatome bei 2,8 MeV Energie der He⁺-Ionen wurde beobachtet.

1. Introduction

Rutherford backscattering and channeling of MeV ⁴He⁺ ions has been successfully applied to the analysis of silicon oxide, silicon nitride and aluminum oxide layers [1 to 3]. This technique has advantages compared with, for example, the weighing method for thin layer analysis, as it is nondestructive and also gives the concentration and depth distribution of all components in the layers. In this paper we discuss the analysis of phosphosilicate glass (PSG) layers by the backscattering technique. PSG layers are of great importance in semiconductor device technology as they show enhanced passivating properties, especially by gettering the mobile alkali ions known to cause device instabilities. The gettering properties improve with increasing P concentration and thickness of the PSG layer, although unfortunately polarization effects due to higher P concentration result in new instabilities. These problems have been studied by others, and a review of some aspects of PSG stabilization is given by Balk and Eldridge [4].

In the present analysis, the composition of the PSG layer over thermally grown SiO₂ on Si single crystal substrates has been determined. The amount of silicon and oxygen in the film has been measured before and after PSG forma-

¹⁾ Present address: Dornier-System GmbH, Friedrichshafen, Bodensee.

tion and the influence of P-predeposition time and anneal treatment on composition has been studied. Using an incident beam of 2.8 MeV $^4\text{He}^+$ ions, backscattered particles from P atoms could be well resolved in energy from $^4\text{He}^+$ ions scattered from Si atoms. Further, ^{29}Si and ^{30}Si isotopes could be separated from ^{28}Si . Low concentrations of heavy mass impurities, such as sulphur for example, may be introduced during sample preparation. These impurities will be recorded in the backscattering spectra and can be avoided in further sample handling.

2. Experimental Method

Backscattering and channeling effect measurements have been performed using 1.0, 2.0, and 2.8 MeV $^4\text{He}^+$ ions produced by a Van de Graaff accelerator. The samples were mounted and oriented on a two-axis goniometer. Particles backscattered from these samples were detected by a surface barrier detector with a resolution of 12 keV and the pulses produced were amplified and stored in a multichannel analyser. The energy-to-channel number conversion, determined from particles backscattered from O and Si atoms at the surface of the layer, was for the different energies 1.7, 3.3, and 5.0 keV/channel, respectively. Target currents of about 15 nA were used and secondary electrons were suppressed. Backscattering spectra were made with the same charge incident upon the target, as measured with a current integrator.

Wafers of 5 Ωcm n-type single crystal silicon were cut parallel to the (111) plane, with lapping and polishing producing a thickness of 250 μm . After cleaning, wafers were heated in dry oxygen at 1000 $^\circ\text{C}$ to grow a 1300 Å thick SiO_2 layer. PSG films were prepared by alloying the SiO_2 layers with P_2O_5 . Various glass compositions and thicknesses were produced by varying the alloying temperature (950 $^\circ\text{C}$, 1050 $^\circ\text{C}$, 1150 $^\circ\text{C}$) and growth time. The same furnace and temperature were used for the deposition and annealing process. The phosphorus source employed was PBr_3 and gas flow and concentration were held constant in all experiments. All PSG layers thicknesses were determined by etch rate analysis together with an ellipsometric technique. This meant etching the glass step by step with P etch which is known to be a selective etchant for PSG [5]. The glass-silica interface was detected by a drastic reduction of the etch rate.

3. Analysis

Fig. 1 shows a random and a $\langle 111 \rangle$ aligned spectra produced by 2.8 MeV $^4\text{He}^+$ ions, scattered from a 1315 Å silicon oxide layer which was deposited on $\langle 111 \rangle$ oriented silicon, together with a random spectrum from pure silicon. The scattering yield from the silicon substrate is strongly reduced by aligning the $\langle 111 \rangle$ single crystal axis with the incident beam direction. The peak in the energy range called HW_0 is due to scattering from the oxygen atoms. The height of the peak $R_0(x)$ is proportional to the concentration of the oxygen atoms at depth x of the layer, while the width at half height HW_0 corresponds to the thickness of the layer t . The peak area is proportional to the total number of oxygen atoms in the layer. The proportionality constant $[S]$ between layer thickness t and HW_0 is given by

$$[S] = \alpha \left. \frac{dE}{dx} \right|_{E_1} - \frac{1}{\cos \theta} \left. \frac{dE}{dx} \right|_{\alpha E_1}$$

with α , fractional energy loss due to scattering, θ , scattering angle in laboratory system, E_1 , energy of incident particles, dE/dx , specific energy loss at energies E_1 and αE_1 . Then

$$HW_0 = t [S] \tag{1}$$

gives the conversion from energy to depth scale. If the layer thickness t is known, e.g. from ellipsometric measurements, then the $[S]$ -value can be calculated.

The part of the spectrum in the energy range called ΔE_{Si} corresponds to scattering from silicon atoms in the oxide layer. In analogy to the discussion of the oxygen peak, ΔE_{Si} corresponds to the layer thickness t , while $R_{Si}^{SiO_2}$ is proportional to the concentration of Si atoms in SiO_2 . Thus the conversion from energy loss to depth scale is given by

$$\Delta E_{Si} = t [S_{Si}^{SiO_2}]. \tag{2}$$

The total number of Si atoms in the layer again is proportional to the peak area approximated by the product $\Delta E_{Si} R_{Si}^{SiO_2}$. The subscript in $[S]$ and R denotes the atom, while the superscript indicates the compound in which the $[S]$ - and R -values of this atom can be calculated. Note that the $[S]$ -values for oxygen and silicon in the silicon oxide layer are different.

The height of the random spectrum R_{Si}^{Si} is proportional to the concentration of silicon atoms in the substrate. Generally the scattering yield $R(E) dE$ in the energy interval E to $E + dE$ is proportional to the concentration of particles in a depth element δx and is given by

$$R(E) dE = N(x) \sigma f \delta x, \tag{3}$$

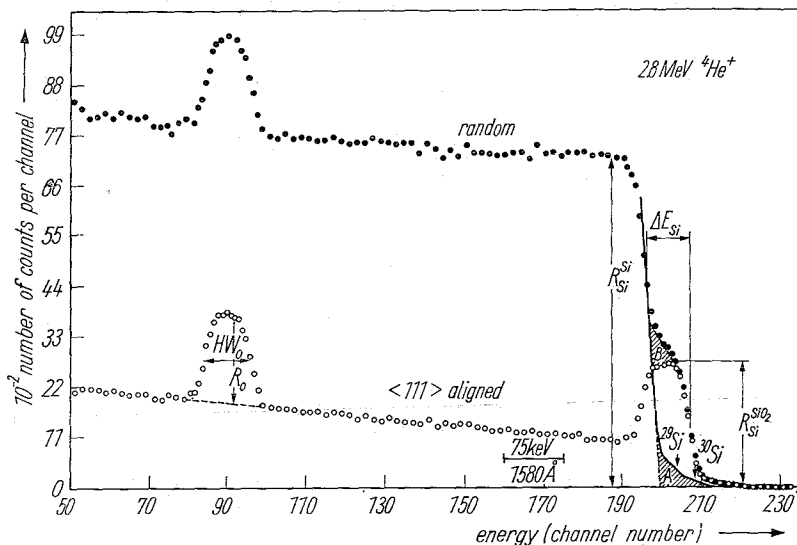


Fig. 1. Random and $\langle 111 \rangle$ aligned spectra of an SiO_2 layer on a single crystal Si substrate. A spectrum of pure silicon shifted in energy to match the silicon substrate edge shows the mass resolution of the Si isotopes (area A). Area A is responsible for the difference in peak heights of Si in the SiO_2 layer in the random and aligned spectra (area B)

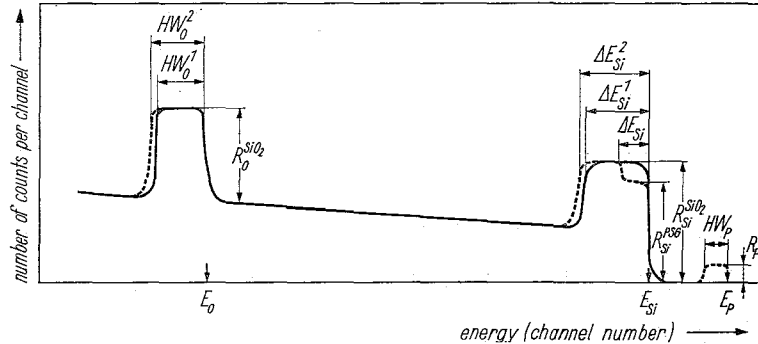


Fig. 2. Schematic diagram of aligned spectra before and after P deposition showing the half widths and heights of the peaks used in this analysis. Solid line SiO_2 , dotted line $\text{SiO}_2 + \text{PSG}$

where f is a proportionality factor for the geometrical arrangement of the experimental system and σ is the Rutherford scattering cross section. Inserting $dE = [S] \delta x$ in (3) results in

$$N(x) = \frac{R(E) [S]}{\sigma f} \quad (4)$$

which gives the concentration of particles at any depth x . There is a significant difference in peak heights of the silicon in the oxide layer in the random and aligned spectra. The reason for this effect is due to the previously mentioned high mass resolution of the 2.8 MeV $^4\text{He}^+$ incident beam, producing the separation of particles scattered from ^{28}Si and ^{29}Si (4.7%) and ^{30}Si (3.1%). In the random spectrum, particles scattered from ^{29}Si and ^{30}Si in the substrate have the same energies as particles scattered from the silicon in the oxide layer and overlap in the spectrum. The same effect occurs in the aligned spectrum, but as the scattering yield from the substrate is strongly reduced, the amount of particles scattered from the Si isotopes in the substrate is negligible. In Fig. 1 a random spectrum from pure silicon, shifted in energy in order to match the substrate edge, is shown for comparison. The scattering yields from the Si isotopes are clearly seen with the dashed areas A and B being approximately equal in size.

Fig. 2 shows a schematic drawing of the backscattering spectrum for a sample aligned with $\langle 111 \rangle$ axis to the incident beam. The solid line indicates the spectrum of the pure oxide SiO_2 whereas the dotted line gives the spectrum of the layer after phosphorus deposition. The small peak below E_P in the high energy part of the spectrum is due to scattering from phosphorus atoms in the PSG film.

Using formulas (1) and (2), respectively, the following relations for the $[S]$ -values for different atoms in the different layers are derived

for oxygen in the SiO_2 layer: $H W_0^1 = t_1 [S_{\text{O}}^{\text{SiO}_2}]$,

for oxygen in the $\text{SiO}_2 + \text{PSG}$ layer: $H W_0^2 = t_2 [S_{\text{O}}^{\text{SiO}_2 + \text{PSG}}]$,

for phosphorus in the PSG layer: $H W_P = t_{\text{PSG}} [S_P^{\text{PSG}}]$,

for silicon in the SiO_2 layer: $\Delta E_{\text{Si}}^1 = t_1 [S_{\text{Si}}^{\text{SiO}_2}]$,

for silicon in the PSG layer: $\Delta E_{\text{Si}}^2 = t_{\text{PSG}} [S_{\text{Si}}^{\text{PSG}}]$,

where t_1 , t_2 , and t_{PSG} are the thicknesses of the oxide layer, the total $\text{SiO}_2 + \text{PSG}$ layer and the PSG layer, respectively.

In general, the $[S]$ -values for O, Si and P in SiO_2 and PSG layer are different. With (4) the following expressions for the concentration ratios are derived:

$$\frac{N_{\text{P}}^{\text{PSG}}}{N_{\text{Si}}^{\text{Si}}} = \frac{R_{\text{P}}^{\text{PSG}}}{R_{\text{Si}}^{\text{Si}}} \frac{[S_{\text{P}}^{\text{PSG}}]}{[S_{\text{Si}}^{\text{Si}}]} \frac{\sigma_{\text{Si}}}{\sigma_{\text{P}}}, \quad (5)$$

$$\frac{N_{\text{Si}}^{\text{PSG}}}{N_{\text{Si}}^{\text{Si}}} = \frac{R_{\text{Si}}^{\text{PSG}}}{R_{\text{Si}}^{\text{Si}}} \frac{[S_{\text{Si}}^{\text{PSG}}]}{[S_{\text{Si}}^{\text{Si}}]}, \quad (6)$$

$$\frac{N_{\text{O}}^{\text{SiO}_2}}{N_{\text{Si}}^{\text{SiO}_2}} = \frac{R_{\text{O}}^{\text{SiO}_2}}{R_{\text{Si}}^{\text{SiO}_2}} \frac{[S_{\text{O}}^{\text{SiO}_2}]}{[S_{\text{Si}}^{\text{SiO}_2}]} \frac{\sigma_{\text{Si}}}{\sigma_{\text{O}}}. \quad (7)$$

The calculated σ ratios for our experimental arrangement ($\theta = 168^\circ$) are

$$\frac{\sigma_{\text{Si}}}{\sigma_{\text{O}}} = 3.34; \quad \frac{\sigma_{\text{Si}}}{\sigma_{\text{P}}} = 0.86; \quad \frac{\sigma_{\text{P}}}{\sigma_{\text{O}}} = 3.86$$

with the subscripts and superscripts in N being used in the same way as for R and $[S]$.

If an absolute concentration, for example for Si in substrate material, is known, then other concentrations can be calculated.

4. Results

From the thickness measurements, together with the measured values of HW_{O}^1 , HW_{P} , ΔE_{Si}^1 , ΔE_{Si} the following $[S]$ -values in eV/Å were calculated for 2.0 and 2.8 MeV $^4\text{He}^+$ in SiO_2 and PSG:

	2.0 MeV	2.8 MeV
$S_{\text{O}}^{\text{SiO}_2}$	40.9	43.7
$S_{\text{O}}^{\text{SiO}_2+\text{PSG}}$	41.8	44.8
$S_{\text{O}}^{\text{SiO}_2}$	47.2	46.7
$S_{\text{Si}}^{\text{PSG}}$	49.5*)	47.4
$S_{\text{P}}^{\text{PSG}}$	44.4	46.0

*) Value for $S_{\text{Si}}^{\text{SiO}_2+\text{PSG}}$.

These results show that there is no great difference in the stopping powers of SiO_2 and PSG. This is due to the small difference in the atomic numbers of Si and P and to the relative low P content in the PSG layer.

In Fig. 3, as an example, typical $\langle 111 \rangle$ aligned spectra before and after P deposition (for 4 min at 1050 °C) are shown.

In the untreated spectrum it can be seen that, using a 2.8 MeV $^4\text{He}^+$ analysing beam, the mass resolution is high enough to separate the Si isotopes at the front edge. After P deposition, the aligned spectrum shows a well resolved P peak, a step in the front edge of the Si peak and an increase in the widths of the Si and oxygen peaks. No increase in the dechanneling rate has been observed; we have estimated that a possible increase is within the statistical error of our measurements. Background correction has to be applied for the P-peak by subtracting the scattering yield due to scattering from the Si isotopes. The plateau of the peak is not influenced by system resolution, as was verified by tilting the

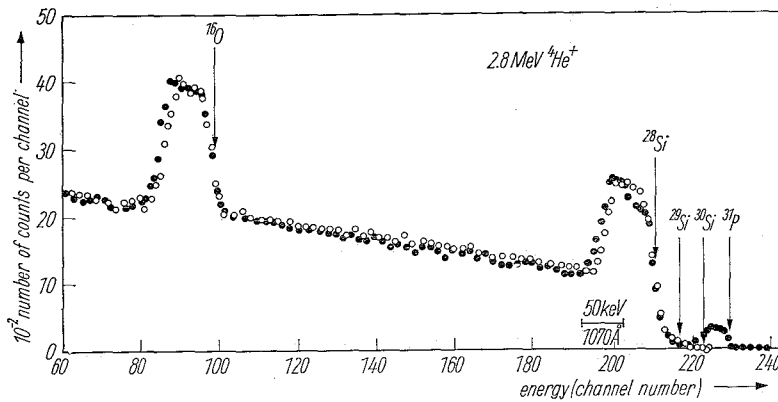


Fig. 3. Aligned spectra ($\langle 111 \rangle$) obtained from a layer before and after P deposition. The characteristics of the spectrum of the treated layer are a well resolved P peak in the high energy part of the spectrum, a step in the Si peak and an increase in the half width of the silicon and oxygen peaks. \circ SiO_2 untreated, \bullet 4 min P deposition at 1050°C

surface normal 70° off incident beam direction. This increases the layer thickness by a factor of about three and the same relative plateau height was found for the P-peak. The height of this plateau corresponds to the maximum concentration of phosphorus in SiO_2 at 1050°C for 4 min deposition time. The absolute concentration of P can be determined by relating this plateau height to $R_{\text{Si}}^{\text{Si}}$, the height of the substrate front edge of the random spectrum shown in Fig. 1. Values for $[S_{\text{Si}}^{\text{Si}}]$ of $44.9 \text{ eV}/\text{\AA}$ and $40.5 \text{ eV}/\text{\AA}$ for 2.0 and 2.8 MeV as calculated from data given by Eisen et al. [6] were used. From (5) with $N_{\text{Si}}^{\text{Si}} = 5 \times 10^{22} \text{ Si}/\text{cm}^3$ we obtain $0.25 \times 10^{22} \text{ P}/\text{cm}^3$ in the PSG layer as the maximum concentration at 1050°C . At shorter P-deposition times, where thinner PSG layers are formed, the P peak in the backscattering spectra does not reveal a plateau. In these cases the concentrations have been determined from peak areas and the thicknesses of the layers, the latter being obtained from the interferometric measurements. Phosphorus concentrations were found to increase from $1.0 \times 10^{21} \text{ P}/\text{cm}^3$ to $2.5 \times 10^{21} \text{ P}/\text{cm}^3$ with increasing deposition time between 30 s and the maximum value of 240 s at 1050°C .

In Fig. 4 P peaks are shown for 4 min deposition time and different deposition temperatures. At 1150°C the maximum concentration value is 36% lower than the value at 1050°C . This is in agreement with the existing phase diagram of the $\text{SiO}_2\text{-P}_2\text{O}_5$ system [8], for the absolute concentrations however we find a deviation by a factor of about two. From our numerical data we obtain 6 mol% P_2O_5 in the PSG layer at 1050°C , whereas 12 mol% are found from the phase diagram. As we achieved good agreement in phosphorus concentration from peak height and peak area measurements and as the errors in measured and calculated $[S]$ -values are not greater than 10% the deviations from the phase diagram are thought to be due to the relatively short deposition times. An appreciably lower P content in PSG layers than indicated by the phase diagram has also been reported by Kooi [9] for short deposition times ($< 15 \text{ min}$) and for low temperatures. The peak at 950°C showing too low a value for the phosphorus concentration is in agreement with these results of Kooi.

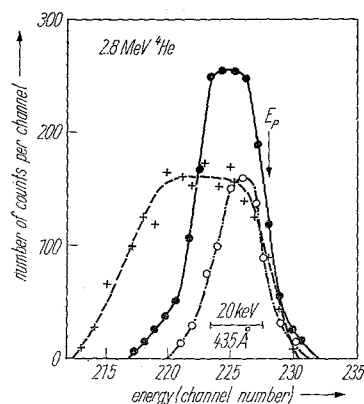


Fig. 4

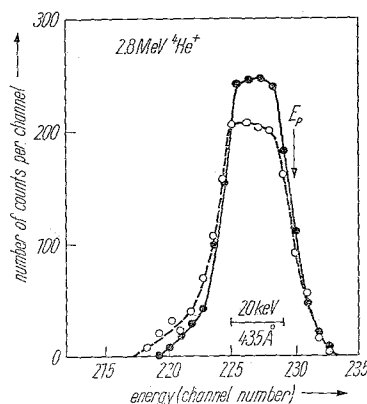


Fig. 5

Fig. 4. Phosphorus peaks after 4 min deposition at 1150 (+), 1050 (●) and 950 (○) °C. Thicker PSG layers are formed at higher deposition temperatures for the same deposition time.

Fig. 5. Phosphorus peaks after 4 min deposition at 1050 °C before and after anneal treatment in N_2 atmosphere. The decrease in P peak height after annealing indicates phosphorus out-diffusion. ● 4 min, 1050 °C; ○ 4 min, 1050 °C and 40 min at 1050 °C in N_2 .

The influence of post anneal treatment in N_2 atmosphere at 1050 °C on the P peak is presented in Fig. 5. The reduction in peak height is due to out-diffusion of phosphorus, and although the increase of the low energy tail may indicate a P in-diffusion, this increase does not compensate the total loss of P atoms. A small loss of O atoms was also observed during post anneal treatment.

Because $[S_{Si}^{SiO_2}]$ is nearly equal to $[S_{Si}^{PSG}]$ the increase of the Si peak width as shown in Fig. 3 is due to an increase of total layer thickness. For this same reason the reduced height of the step is due to a reduced Si concentration in the PSG layer. From (6) this concentration was calculated to be 1.9×10^{22} Si/cm³ at 1050 °C; in the pure oxide layer a value of 2.2×10^{22} Si/cm³ was found.

The oxygen peak shows an increase in half width, and as the $[S]$ -values $[S_{O}^{SiO_2}]$ and $[S_{O}^{SiO_2+PSG}]$ are also approximately equal, this indicates an increase of the layer thickness. Within our experimental error no change of the oxygen peak height was observed, which suggests that the O concentration is approximately the same in PSG and in SiO_2 . From (7) a value for this oxygen concentration of 4.56×10^{22} O/cm³ was calculated. From the absolute Si and O concentrations calculated from the 2 MeV spectra the oxygen to silicon ratio in the untreated samples is 2.07, whereas from total peak area measurements a value of 1.97 has been calculated. These deviations are within our experimental error and may be due to statistical fluctuations in the peak heights.

For the oxygen to silicon ratio determined from spectra using 2.8 MeV $^4He^+$ ions values of about 2.3 have been calculated. This deviation from stoichiometry was found to be due to enhanced scattering from the oxygen atoms at this incident energy. Oxygen and silicon peak areas were carefully measured and normalized to the random spectra for energies at 1.0, 2.0, and 2.8 MeV.

The following relative values were obtained for silicon: 635, 626, 645 and for oxygen: 345, 368, and 430. This value of 430 for oxygen at 2.8 MeV which is much greater than those at 1 and 2 MeV is well outside the calculated error of

measurement. This enhanced scattering is thought to be due to cross section enlargement by resonance scattering as suggested by Mayer [7]. Further investigations are being conducted to obtain more quantitative data about this effect.

If a mean value of 2.02 for the oxygen to silicon ratio is assumed to be present in the PSG layer, then the oxygen to phosphorus ratio in this layer can be calculated, i.e. $N_O/N_P = (4.56 - 1.9 \times 2.02) \times 10^{22} / 0.25 \times 10^{22} \approx 2.8$. From this value which has an error of about 30% it is assumed that stoichiometric P_2O_5 has been incorporated into the PSG layer.

The ratio of oxygen to phosphorus atoms can be determined independently by peak area measurements from

$$\frac{N_O}{N_P} = \frac{\Delta F_O}{F_P} \frac{\sigma_P}{\sigma_O},$$

where ΔF_O is the increase of the oxygen peak area proportional to the amount of O atoms absorbed during deposition and F_P is the area of the P peak in the spectra.

Using this formula the average ratio of incorporated O and P atoms was found to be about four. This higher value probably arises from additional oxygen incorporation due to silicon oxide growth during deposition. The observation of additional oxide growth is supported by an increase of the total Si peak area after deposition. From this increase a growth of about 50 Å of additional SiO_2 can be estimated.

5. Conclusions

As 2.8 MeV $^4He^+$ ions backscattered from P and Si atoms are well separated in the backscattering energy spectra, it is possible to analyse the composition of PSG layers on SiO_2 by backscattering and channeling effect measurements.

As special effects in the backscattering technique can occur for certain atomic species at specific energies, care has to be taken in concentration determination for these atoms. Cross section enlargement for scattering from oxygen atoms at 2.8 MeV $^4He^+$ has been reported in this paper.

Additional oxide growth during P deposition has been detected and the thickness of this oxide layer has been estimated.

An estimate of the P to O ratio incorporated during deposition has been given; the reported value shows that the assumption of a $SiO_2-P_2O_5$ composition of PSG layers, made in analysis using weighing and etching techniques is probably justified.

References

- [1] O. MEYER, J. GYULAI, and J. W. MAYER, *Surface Sci.* **22**, 263 (1970).
- [2] O. MEYER and W. SCHERBER, *J. Phys. Chem. Solids* **32**, 1909 (1971).
- [3] I. V. MITCHELL, M. KAMOSHIDA, and J. W. MAYER, *Appl. Phys. Letters* **18**, 292 (1971).
- [4] P. BALK and J. M. ELDRIDGE, *Proc. IEEE* **57**, 1558 (1969).
- [5] W. A. PLISKIN and R. P. GNALL, *J. Electrochem. Soc.* **111**, 872 (1964).
- [6] F. H. EISEN, G. J. CLARK, J. BÖTTIGER, and J. M. POATE, *Radiat. Eff.* **13**, 93 (1972).
- [7] J. W. MAYER, private communication.
- [8] T. Y. TIEN and F. HUMMEL, *J. Amer. Ceram. Soc.* **45**, 422 (1962).
- [9] E. KOOL, *J. Electrochem. Soc.* **111**, 1383 (1964).

(Received January 31, 1973)